Impact of Radiometric Calibration and Specifications of Spaceborne Optical Imaging Sensors on the Development of Operational Automatic Remote Sensing Image Understanding Systems

Andrea Baraldi

***Abstract*—The development of operational automatic remote sensing (RS) image understanding systems (RS-IUSs) represents a traditional goal of the RS community. Unfortunately, to date, the transformation of huge amounts of multisource, multiresolution Earth observation (EO) imagery into information still remains far below reasonable expectations. The original contribution of this work to existing knowledge on the subject of automating the quantitative analysis of EO images is fourfold. *In primis* this paper moves from existing literature to consider the radiometric calibration of RS images a *necessary, although not sufficient*, condition for implementation of operational automatic RS-IUSs. This requirement complements the traditional perception of calibration and validation (Cal/Val)-related activities as crucial in achieving harmonization and interoperability of multisource EO data and derived information products generated at all scales as envisaged under: (i) the Global Monitoring for the Environment and Security (GMES) project, led by the European Union (EU), and (ii) the Global Earth Observation System of Systems (GEOSS) program, conceived by the Group on Earth Observations (GEO) whose space arm, the Committee of Earth Observations (CEOS), recently delivered a Quality Assurance Framework for Earth Observation (QA4EO) data. The second objective of this paper is to solicit the RS community to further investigate the calibration quality and uncertainty of the well-known Satellite Pour l'Observation de la Terre (SPOT) and Indian Remote sensing Satellite (IRS) imaging sensor series whose zero-value offset parameters appear questionable based on experimental evidence. Third, this work provides a quantitative assessment of the spectral information loss that, in comparison with the ongoing SPOT-4/-5 optical sensors, may affect future planned European EO satellites such as Pleiades-1/-2 and the follow-on missions Astrium SPOT-6/-7. Finally, this work shows that, in several recent or ongoing scientific applications of EO images acquired across time, space, and sensors, the mandatory radiometric calibration preprocessing stage appears to be surprisingly ignored or underestimated by EU space agencies and research institutions that have been members of the CEOS for more than twenty years and should be eager to transform the new QA4EO initiative into RS common practice.**

***Index Terms*—Image understanding system, operational performance measurement, radiometric calibration into top-of-atmosphere (exoatmospheric planetary) radiance/reflectance values.**

Manuscript received November 14, 2008; revised May 12, 2009. Current version published September 09, 2009.

The author was with the European Commission Joint Research Centre, I-21020 Ispra (Va), Italy. He is now with Baraldi Consultancy in Remote Sensing, 40129, Bologna, Italy (e-mail: andrea6311@gmail.com).

Color versions of one or more of the figures in this paper are available online at http://ieeexplore.ieee.org.

Digital Object Identifier 10.1109/JSTARS.2009.2023801

I. Introduction

In recent years, the number and performance of spaceborne optical sensors for Earth observation (EO) has continued to increase together with the demand for remote sensing (RS) observational data, metadata and derived information products [1]–[4]. The impact of spaceborne optical imagery upon scientists and decision-makers around the world has recently profited from unrestricted access at no charge to large-scale low- and medium-resolution RS image archives [5]. These multiple drivers make urgent the need to develop operational satellite-based measurement systems suitable for automating the quantitative analysis of RS imagery, which is one of the traditional goals of the RS community involved with global land cover and land cover change assessment [1].

Unfortunately, to date existing scientific and commercial RS image understanding systems (RS-IUSs) [6] score low in operational performance [7]–[9]. As a consequence, the transformation of huge amounts of multisource, multiresolution spaceborne imagery into information still remains far below reasonable expectations and mostly confined to scientific rather than operational applications [10]. This may be due to both theoretical and technological lacks in existing knowledge on the subject of RS image understanding.

- From a conceptual point of view, any imaging sensor projects a (3-D) scene onto a (2-D) image. Therefore, the main role of a biological or artificial image understanding system is to back-project the sub-symbolic information in the (2-D) image domain onto the symbolic information in the (3-D) scene domain. This means that the problem of image understanding is inherently ill-posed and consequently very difficult to solve [11]. The inherent ill-posedness of image understanding is the same as that of inductive learning. Starting from classical philosophy to end up with machine learning it is well known that the general notion of inference (learning) comprises two types of learning mechanisms known as "induction (i.e., progressing from particular cases [e.g., training data] to general [e.g., estimated dependency or model])", therefore called bottom-up, fine-to-coarse, data-driven, or learning-by-example, and "deduction (i.e., progressing from general [e.g., model] to particular

cases [e.g., output values])", therefore called top-down, coarse-to-fine, model-driven, or learning-by-rule [12]. In particular, "induction amounts to forming generalizations from particular true facts. This is an inherently difficult (ill-posed) problem and its solution requires *a priori* knowledge in addition to data" [12, p. 39].

- From a technical viewpoint, a data processing system is automatic when it requires no user-defined parameter to run; therefore, its ease of use is unsurpassed. *In automating a data processing system, necessary, although not sufficient, conditions are for input data to be* [13]: (i) well behaved (well conditioned), i.e., not violating any assumptions needed to successfully apply whatever analysis the system performs, e.g., every input data source is expressed in a physical unit of measure and belongs to a known domain of variation and (ii) well understood by the system developer, namely, every input data source is provided with a clear physical meaning and with a community-agreed data format.

Based on the foregoing considerations and in line with machine learning [14], computer vision [11], RS literature [13], [15], [16], and common sense (synthesized by the expression: "garbage in, garbage out"), RS-IUSs should increase their degree of automation by making stronger assumptions about the input dataset (equivalent to prior knowledge of the real world, known as the *world model* [11]) to make it well behaved and well understood. On the contrary, most (if not all) existing RS-IUSs:

- Do not require RS images to be: (a) radiometrically calibrated, i.e., they do not require dimensionless digital numbers (DNs) to be transformed into a radiometric unit of measure, and (b) validated in terms of unequivocal geometric and radiometric quality. As a consequence these RS-IUSs adopt a manual or, at best, semi-automatic data understanding approach on a scene-by-scene basis (since one scene may represent, say, apples while a contiguous or overlapping scene may represent, say, oranges).[1]

- Provide RS experts and practitioners with overly complicated inductive data learning options to choose from based on scene-specific heuristic criteria.

As a consequence, these RS-IUSs are difficult to use and unsuitable for mapping large-scale RS datasets requiring an automatic data product generation and delivery chain.

The original contribution of this work to existing knowledge on the development of operational automatic RS-IUSs is fourfold. Starting from existing literature this paper considers the availability of radiometrically calibrated spaceborne optical imagery of validated geometric and radiometric quality *conditio sine qua non* for development of operational automatic RS-IUSs robust to changes in the input RS data acquired across time, space and sensors.

It is noteworthy that calibration and validation (Cal/Val)-related activities are traditionally considered crucial in achieving harmonization and interoperability of EO data and derived information products generated from a variety of sources at all scales-global, regional and local-as envisaged under the visionary goal of the Global Earth Observation System of Systems (GEOSS), conceived by the Group on Earth Observations (GEO)[2] [17], [18]. In the context of a GEOSS, an appropriate coordinated program of Cal/Val activities throughout all stages of a spaceborne mission, from sensor build to end-of-life, is considered mandatory by the Quality Assurance Framework for Earth Observation data (QA4EO) [19], led by the Committee of Earth Observations (CEOS)[3] [20] Working Group on Calibration and Validation (WGCV)[4] [21]. A continuous traceable Cal/Val activity, well defined and controlled through common standards, is also required by the Global Monitoring for the Environment and Security (GMES) program, led by the European Union (EU) in partnership with the European Space Agency (ESA), to guarantee the sustainability of integrated operational services for EU security and environmental monitoring based

[1]To the best of the author's knowledge, no other scientific field like RS relies, on a regular basis, on measures provided with no unit of measure belonging to an international system of units. If Rome was not built in one day, could Rome be built in one thingamabob? When the question is fuzzy (garbage in), the sole possible answer is "maybe" (garbage out).

[2]GEO was launched in response to calls for action by the 2002 World Summit on Sustainable Development and by the G8 (Group of Eight) leading industrialized countries [17]. GEO provides a framework for the coordination of efforts and strategies to address common goals in EO. It comprises a voluntary partnership of 77 governments and the European Commission (EC), in addition to 56 intergovernmental, international, and regional organizations with a mandate in EO or related issues that have been recognized as Participating Organisations. In 2005 GEO launched a "ten-year implementation plan" to establish its visionary goal of a global EO system of systems, GEOSS [18].

[3]CEOS was created in 1984 in response to a recommendation by the Economic Summit of Industrialized Nations Working Group on Growth, Technology, and Employment's Panel of Experts on Satellite Remote Sensing [20]. This group recognized the multidisciplinary nature of satellite EO and aims at optimizing benefits of spaceborne EO through cooperation among its participants in mission planning and in development of compatible data products, formats, services, applications and policies. CEOS became the space arm of GEO in 2006. In that capacity, CEOS is playing an active role in the establishment of GEOSS. CEOS members are, among others: Agenzia Spaziale Italiana (ASI), British National Space Centre (BNSC), Centre National d'Etudes Spatiales (CNES), Deutsches Zentrum für Luft- und Raumfahrt (DLR), European Commission (EC), European Space Agency (ESA), European Organization for the Exploitation of Meteorological Satellites (EUMETSAT), National Aeronautics and Space Administration (NASA), National Oceanic and Atmospheric Administration (NOAA), Canadian Space Agency (CSA), Instituto Nacional de Pesquisas Espaciais (INPE) and Indian Space Research Organization (ISRO).

[4]Initiated in 1984, the CEOS Working Group on Calibration and Validation (WGCV) pursues activities to coordinate, standardize and advance calibration and validation of EO missions and their data in the conviction that the space agencies and commercial satellite data providers should present EO data in a way that would ensure the possibility of comparing sensors and products [21]. Thus, CEOS WGCV, in partnership with the Institute of Electrical and Electronics Engineers (IEEE), was the natural GEO choice to carry out the task of developing an international Quality Assurance Framework for Earth Observation data (QA4EO) in the context of GEOSS. Started in two GEO/CEOS workshops held in 2007 and 2008, the ongoing QA4EO initiative is conceived as an international EO Cal/Val community-derived process to establish an international quality assurance framework to facilitate harmonization and interoperability of EO data, metadata, derived information products, and operations required to achieve them [19].

on EO data from multiple sources (satellite, airborne and in situ) and synergistic data products[5] [22].

To summarise, the first objective of this work is to emphasize that an appropriate coordinated Cal/Val process must be considered mandatory, first, to guarantee the harmonization and interoperability of multisource, multiresolution EO data as envisaged by the GEOSS and GMES programs and, second, to provide the GEOSS and GMES instantiations with operational automatic RS-IUS components. As a consequence, this paper delivers a timely reminder to the space agencies and commercial satellite industries of their responsability to provide the RS community involved with the development of operational satellite-based measurement systems with radiometrically calibrated EO images of validated geometric and radiometric quality.

The second objective of this paper is to solicit further scientific investigation at institutional level of the calibration quality and uncertainty of the well-known Satellite Pour l'Observation de la Terre (SPOT) and Indian Remote sensing Satellite (IRS) imaging sensor series whose zero-value offset parameters appear questionable based on experimental evidence.

The third contribution of this work is to provide a preliminary estimate of the spectral information loss that, in comparison with the ongoing SPOT-4/-5 optical sensors, may affect future planned European EO satellites, such as Pleiades-1/-2 and the follow-on missions Astrium SPOT-6/-7, whose finer spatial resolution is counterbalanced by a change in spectral resolution that increases their interband data correlation and sensitivity to the presence of haze and aerosols.

Finally, this paper shows that in several recent or ongoing scientific applications of EO images, acquired across time, space and sensors, focused on global land cover mapping and land cover change detection, risk management and fast reaction to catastrophic events, the mandatory radiometric calibration preprocessing stage appears to be surprisingly ignored or underestimated by EU space agencies and research institutions that have been members of the CEOS for more than twenty years and which should be eager to transform the new QA4EO initiative into RS common practice. This means that, in spite of their international commitment to accomplish Cal/Val-related activities for EO data quality assurance, EU space agencies and research institutions may be slow, reluctant or inadequate in moving from scientific to operational EO data applications.

The rest of this paper is organized as follows. Section II provides the scientific background and definitions useful in relating the development of operational automatic RS-IUSs to the visionary goals of the GEOSS and GMES programs which require harmonization and interoperability of EO data derived from a variety of sources. Section III surveys related works on the subjects of RS data radiometric calibration, atmospheric correction and existing operational automatic RS-IUSs. Starting from experimental evidence, Section IV investigates the effectiveness and reliability of the absolute radiometric calibration zero-value offset parameters adopted by the well-known SPOT and IRS imaging sensor series. Section V compares the radiometric calibration capabilities of European versus non-European EO satellite optical sensors. In Section VI, additional sensor specifications causing an increase in the timeliness of either ongoing or future EU satellite optical missions are discussed. Section VII provides examples of several small- and large-scale research and development projects where EU space agencies and scientific institutions ignore the radiometric calibration preprocessing requirement and extract information on a scene-by-scene basis from RS images acquired across time, space and sensors. Conclusions are reported in Section VIII.

II. Scientific Background and Definitions

This section provides the scientific background and definitions useful in relating the development of operational automatic RS-IUSs suitable for use in large-scale multisource, multiresolution spaceborne optical image archives to the visionary goals of the GEOSS and GMES programs which require a coordinated plan of standardized Cal/Val activities to guarantee harmonization and interoperability of EO data generated from a variety of sources.

The potential of the increasing amount of RS imagery acquired from multiple platforms for the monitoring of the earth's environment and detection of its temporal variations at geographic extents ranging from local (areas up to 100 000 km^2) to regional (areas roughly between 100 000 and 1 000 000 km^2), continental and global scales is well known by user communities involved with urban growth assessment and planning, property tax assessment, intelligence/surveillance applications for national security and defense purposes, tourism, ecosystem management, watershed protection, water balance calculations, risk management and global change [1]–[4].

The traditional use of EO data for environmental monitoring is expected to be revolutionized by universal availability of cost-free large-scale low—(above 40 m) and medium—(from

[5]ESA is the coordinator of the space component of GMES and is ensuring the flow of EO data into the GMES services along with access to these data [23]. As a primary recipient of EO data, the EC has identified five initial GMES Core Services projects, including three fast-track services focusing on land, marine and emergency services and two pilot service projects focusing on security and atmospheric composition. Preoperational data provision to the five GMES Core Services projects is planned to begin before the end of 2008. In 2008, ESA received 12 proposals offering to provide, over the next few years, GMES Services with RS data acquired from more than 40 European and non-European EO satellites. Thus, the fleet of GMES contributing missions is constantly increasing. Among other satellites there are ESA Member States' missions, such as France's SPOT and Pleiades satellites, Germany's 5-satellite RapidEye constellation and TerraSAR-X, Italy's CosmoSkyMed, the UK-led Disaster Monitoring Constellation (DMC) (including the soon-to-be launched DMC-UK2 and Spain's Deimos-1), as well as Canada's Radarsat, Israel's EROS and other non-European missions distributed through European companies such as the FORMOsa SATellite (FORMOSAT)-2 and the KOrean MultiPurpose SATellite (KOMPSAT)-2. In addition, ESA will act as data provider for its own EO missions, such as Envisat and ERS-2, as well as its Third Party Missions such as the Project for On-Board Autonomy (PROBA). ESA and the European Organisation for the Exploitation of Meteorological Satellites (EUMETSAT) offer their data free of charge, while other agencies offer favourable conditions to the GMES Services. Thanks to harmonized protocols and standards developed by EU space agencies through the Heterogeneous Mission Accessibility (HMA) Project, ESA is able to harmonize data flow and data access. Moreover, to ensure that GMES Services have quick, easy and coherent access to data from all of the missions, ESA will provide a dedicated Data Access Portal where GMES Services can obtain relevant information and access the data products. Many of these data sets will be distributed relying on the operators of contributing satellite missions.

40 to 20 m) spatial resolution spaceborne optical image archives. GEO recently announced that scientists and decision-makers around the world will soon have unrestricted access at no charge to the Landsat archive, the world's most extensive collection of continuously-acquired RS spaceborne imagery [5]. This news followed the decision by the China-Brazil Earth Resources Satellite (CBERS) to distribute its images free of charge starting from the year 2007. In turn, the EU announced a free data policy for the Sentinel-2/-3 satellites whose launch is scheduled starting from 2012.

While the cost-free access to large-scale low- and medium-spatial resolution RS image databases is becoming a reality, the demand for very high spatial resolution (VHR, below 5 m resolution) commercial satellite imagery has continued to increase in terms of both quantity and quality of data. For example, the United States government spent \$5–6 M in 1991 and \$200 M in 2003 for the purchase of VHR satellite images [4]. The increasing request for VHR spaceborne imagery has boosted the rapid growth of the commercial VHR satellite industry. For example, within the year 2012 ongoing VHR spaceborne optical imaging sensors, such as GeoEye-1, QuickBird-2, IKONOS-2, OrbView-3, KOMPSAT-2, RapidEye, FORMOSAT-2, and ALOS AVNIR-2, will be joined by future planned VHR spaceborne imaging missions, such as Pleiades-1/-2, WorldView-2 and Astrium SPOT-6/-7.

These multiple drivers solicit the RS community to achieve, in the short- to medium-term, one of the traditional goals of space agencies and scientific and commercial institutions involved with global land cover and land cover change detection programs, such as the Land Use and land Cover Change (LUCC) program and the National Aeronautics and Space Administration (NASA) Land Cover and Land Use Change (LCLUC) program [1, pp. 451, 452], namely, the development of operational satellite-based measurement systems capable of automating the quantitative analysis of multisource, multiresolution RS imagery.

Unfortunately, to date the automatic or semi-automatic transformation of huge amounts of multisource, multiresolution RS imagery into information still remains far below reasonable expectations [10]. For example, the percentage of data ever downloaded by stakeholders from the ESA EO databases is estimated at about 10% [24]. In common practice, insufficient RS image mapping capability may be due to two main factors.

- Existing scientific and commercial RS-IUSs, such as eCognition [6] and the Atmospheric/Topographic correction (ATCOR3) [47], score low in operational performance which encompasses [7]–[9]: (i) ease of use (degree of automation), (ii) effectiveness (e.g., classification accuracy), (iii) efficiency (e.g., computation time, memory occupation), (iv) economy (costs; they increase monotonically with manpower, e.g., the manpower required to collect scene-specific training samples), (v) robustness to changes in input parameters, (vi) robustness to changes in the input dataset, (vii) maintainability/scalability/re-usability to keep up with users' changing needs and (viii) timeliness (defined as the time span between data acquisition and product delivery to the end user; it increases monotonically with manpower). For example, a low operational performance measurement may explain why the impact upon commercial RS image processing software toolboxes of the literally hundreds of so-called novel low (sub-symbolic)- and high (symbolic)-level image processing algorithms presented each year in scientific literature remains negligible [10].
- The increasing rate of collection of RS data of enhanced quality outpaces the capabilities of both manual inspection and inductive machine learning from supervized (labeled) EO data. The cost, timeliness, quality and availability of adequate reference (training/testing) datasets derived from field sites, existing maps and tabular data are considered the most limiting factors on RS data product generation and validation [1], [13], [25]–[30].

To overcome these limitations, well-known keys to operational performance are discussed below [102].

a) Streamline and simplify operations according to structured system design principles capable of enforcing the well-known divide-and-conquer problem-solving approach. To achieve interoperability, structured system design focuses on interfaces between operations. As a consequence, the impact of an individual system operation upon the global system is exactly defined by its interface [18]. In structured system design, any data processing system can be hierarchically described by a data flow diagram (DFD) comprising: (i) operations (processes) as nodes in the DFD, (ii) observational data flows, (iii) derived information flows and (iv) control flows, all represented as oriented edges (equivalent to interfaces) linking nodes in the DFD [7]. It is noteworthy that data processing system design accounts for the customary distinction between a model and the algorithm used to identify it [31], i.e., structured system design defines a data processing system architecture without implementing it. In the words of Page-Jones, "structured system design is everything but code" [7].

b) Standardize operations, observational data, metadata, derived information and control flows [refer to point a) above] in agreement with the QA4EO guidelines [19]. In a DFD, every process and every data/information/control flow must be provided with engineered (quantitative, unequivocal) "reference standards" as a means of evaluating: (i) performance of an activity and (ii) quality of a data flow [32]. Engineered reference standards must take multiple individual evaluation measures into consideration to account for the well-known, but often forgotten in common practice, noninjectivity of any evaluation measure. This means that, for example, different classification maps compared against the same reference sample set may produce the same confusion matrix and that different confusion matrices may generate the same confusion matrix accuracy measure. These observations suggest that no single universally acceptable measure of quality, but instead a variety of indices, should be employed in practice [33], [34]. In the words of the QA4EO initiative, a quality indicator (QI) is based on an unequivocal quantifiable metrological/statistically-based measure [19, p. 7], i.e., a QI is based on a documented

quantitative assessment of its traceability to a community-agreed reference standard ideally tied to a physical unit of measure belonging to an international system of units. In a DFD, QIs belong to the following taxonomy: (i) operation performance index (OPI) equivalent to an operational performance measurement [9], e.g., effectiveness, efficiency, etc., refer to the list of operational system requirements provided above in this text, (ii) observational data quality index (DQI), e.g., geometric and radiometric accuracy of EO sensor derived data, (iii) metadata quality index (MQI), e.g., a declared calibration uncertainty associated with the radiometric calibration parameters, and (iv) derived information product quality index (IQI), e.g., classification and spatial accuracy of a map generated from EO data.

c) Operation performance tracking and data quality monitoring in agreement with the QA4EO guidelines [19]. Accurate operation performance/data quality tracking (traceability) provides knowledge on what is not performing up to a reference standard, so that alternative quality assurance strategies can be enforced at that stage. In line with the QA4EO requirements [19], the term validation can be related to the assignment of unequivocal quantitative OPI/DQI/MQI/IQI values which fall within reference standards to every operation (process), data flow, metadata and derived information product comprised in a EO data product generation and delivery chain.

d) Automating operations. While the abovementioned guiding principle (a) deals with the data processing system architecture, this guideline deals with a data processing system instantiation. An automatic data processing system requires: (I) no user-defined parameter to run, therefore, its ease of use is unsurpassed, and (II) the input data to be [13].

   i) Well behaved (also refer to Section I). EO sensor derived data are well behaved when they are:
      - Radiometrically calibrated, i.e., dimensionless DNs are transformed into a community-agreed radiometric unit of measure.
      - Geometrically corrected, i.e., projected onto a community-agreed terrestrial reference system.
      - Validated, i.e., provided with quantitative, unequivocal and traceable measures of geometric and radiometric EO data quality.
   ii) Well understood by the system developer, i.e., provided with a clear physical meaning and with a community-agreed data format (also refer to Section I).

It is noteworthy that, in the context of the GMES and GEOSS programs [17], [18], [22], and following implementation of the new QA4EO initiative (refer to Section I above), the issue of the Cal/Val activity is expected to quickly climb to the top of space agencies' agendas where it has often ranked low in the past. In the words of an anonymous referee "one of the challenges in the procurement of space instrumentation for RS is balancing the requirements for adequate pre- and postlaunch calibration activities against other project constraints. Calibration usually takes place at the end of an instrument development phase where the pressures of cost and schedule are at their greatest and is often cut short as a consequence. In order to ensure that observational data products are accurately calibrated it is vital that building blocks of a calibrated sensor are incorporated at the outset of instrument development." Notable examples where calibration was one of the most severe requirements of the spaceborne mission are the ENVISAT Advanced Along-Track Scanning Radiometer (AATSR) and the ENVISAT Medium Resolution Imaging Spectrometer Instrument (MERIS) [35].

Traditionally, the biggest obstacles to creating effective onboard calibration systems are the timeliness of the analysis of the hardware requirements, onboard calibration system implementation and integration issues and the project costs which may easily increase with the complexity and degree of novelty of the onboard calibration system. For example, the CEOS WGCV endorses the moon as a reference standard source of luminous intensity for radiometric calibration stability [36], whereas AATSR and MERIS adopt a sun-based onboard calibration device technology which is relatively new and complex to implement [35]. In practice, all spaceborne sensors must rely on continuous vicarious calibration campaigns whose instrument data, site characteristics and implementation periods should be traceable in a common format [19], [37].

To conclude, while QA4EO focuses on Cal/Val activities related to guiding principles (b) and (c) mentioned above and suitable for improving the operational performance of both the GEOSS and GMES system instantiations, the original contribution of this paper is to stress that Cal/Val-related activities are mandatory in automating the quantitative analysis of spaceborne optical imagery in agreement with the data processing system architecture and implementation principles (a) and (d) mentioned above. Overall, this work highlights the (obvious!) fact that an appropriate coordinated program of Cal/Val activities fulfills all the four resolutions (a)–(d) recommended above to improve operational performance of both the GEOSS and GMES system instantiations whose eligible components are operational automatic RS-IUSs.

III. Previous Works

This section provides a summary of related works on the following subjects.

- Radiometric calibration of DNs into: (i) (planetary, exoatmospheric) top-of-atmosphere (TOA) radiance (TOARD), (ii) TOA reflectance (TOARF) and (iii) surface reflectance ρ values when atmospheric effects are removed from either TOARD or TOARF values.
- Operational automatic RS-IUS architectures and implementations that require as input RS images radiometrically calibrated into TOARF values.

A. Radiometric Calibration and Atmospheric Correction

Radiometric calibration, the transformation of dimensionless DNs into a unit of measure related to a community-agreed radiometric scale, comprises a sequence of three steps.

1. Transformation of DNs into nonnegative TOARD values ≥ 0. This first calibration step is also known as *absolute radiometric calibration* [40].

2. Transformation of TOARD values into TOARF values belonging to range [0, 1].
3. When atmospheric effects are taken into account, transformation of either TOARD or TOARF values into surface reflectance ρ values belonging to range [0, 1]. Unfortunately, the problem of atmospheric correction is typically ill- or poorly-posed. Consequently, it is very difficult to solve and requires user's supervision to make it better posed [47].

Although often ignored in common practice by RS scientists and practitioners, radiometric calibration achieves the following objectives (see 1 and 2 above).

- ∘ Acknowledged by existing literature, it ensures the harmonization and interoperability of multisource observational data and derived products required by international programs such as the GEOSS and the GMES [17], [18], [22].
- ∘ According to this work (refer to Sections 1 and 2 above), it makes RS data well behaved and well understood [13], which paves the way to automating the quantitative analysis of EO data [38], [39].

Absolute radiometric calibration [40] is the linear transformation of a pixel value, $\mathrm{DN}(n,b)$, with $n = 1,\ldots,N, b = 1,\ldots,Bnd$, where N is the total number of pixels and *Bnd* is the number of spectral channels (bands), into a TOARD value, $\mathrm{TOARD}(n,b) \geq 0$, expressed in a radiometric unit of measure, either [W/(m$^2\times$ sr $\times\mu$m)] (e.g., Landsat, SPOT, ASTER, QuickBird) or [mW/(cm$^2\times$ sr $\times\mu$m)] (e.g., IKONOS, IRS) [47], as a function of the offset and gain calibration parameters to be retrieved from the RS metadata files. For example, in the case of SPOT-1/-5 imagery [41]

$$0 \leq \mathrm{TOARD}(n,b) = [\mathrm{DN}(n,b)/\mathrm{A}(b)] + \mathrm{B}(b) \quad n = 1,\ldots,N, b = 1,\ldots,Bnd \quad (1)$$

where, for example, $\mathrm{DN}(n,b) \in \{0,255\}$ and $\mathrm{A}(b) \geq 0$ and $\mathrm{B}(b) \geq 0$ are the absolute calibration gain and offset parameters for band b, identified respectively as "⟨PHYSICAL_GAIN⟩" and "⟨PHYSICAL_BIAS⟩" in the SPOT metadata DIMAP file format.

The model for obtaining dimensionless true terrain reflectance, $\rho(n,\lambda,t,\mathrm{lat},\mathrm{long}) \in [0,1]$, from the spectral radiance at the sensor's aperture $\mathrm{TOARD}(n,\lambda)$ may be expressed as [42] shown in (2), at the bottom of the page, where λ is the electromagnetic wavelength; (lat, long) is the pixel position in geographic coordinates; $d(t)$ is the earth-sun distance in astronomical units to be interpolated from values found in literature as a function of the viewing day and time, t, transformed into a Julian day value in range $\{1, 365\}$, such that $d(t)$ approximately belongs to range $1\pm3.5\%$ [43]; $L_a(\lambda) \geq 0$ is the *atmospheric upwelling radiance* scattered at the sensor by the atmosphere (called *airlight* [44], equivalent to an additive term to be assessed by dark-object subtraction techniques: if, by definition of a dark object, $\rho = (2) = 0$, then the unknown variable *La* is equal to the measured TOARD value [45]); $E_d(n,\lambda) \geq 0$ is called *diffuse irradiance at the surface* [42], *ambient light*, or *indirect illumination* [46], contains no information on the surface properties of the pixel and comprises two components: (a) in nonflat terrain areas, light is reflected from other objects (e.g., adjacent slopes in rugged terrain) before being reflected from the pixel under consideration; this first component is called *reflected terrain radiance* and is null in flat terrain [47]; or (b) in both flat and rugged terrain, radiation is reflected from the neighbourhood of the pixel under consideration and, next, it is scattered by the atmosphere into the viewing direction; this second component is called *skylight* [44] or *adjacency radiance* [47]; overall, $E_d(\lambda)$ changes with wavelength and can provide a relevant contribution to incident radiance [42], [45]; $\tau_{\mathrm{uw}}(\lambda) \in [0,1]$ and $\tau_{\mathrm{dw}}(\lambda) \in [0,1]$ are, respectively, the *path atmospheric transmittances of the upwelling* (ground surface-sensor path) and *downwelling* (sun-ground surface path) *flows*; $\mathrm{ESUN}(\lambda)$ is the mean solar exoatmospheric (TOA, planetary) irradiance found in literature [43] (e.g., in the SPOT metadata DIMAP file format, parameter $\mathrm{ESUN}(\lambda)$ is identified as "⟨SOLAR_IRRADIANCE_VALUE⟩"); $\theta_z \in [0,90°]$ is the sun's zenith angle in degrees, typically provided in the image metadata file or computed from the data acquisition time t and per scene or pixel-based lat-long coordinates; term $[\mathrm{ESUN}(\lambda)\cdot\cos(\theta_z)]$ is called sunlight [44] or direct illumination [46] and represents the only radiation component reflected from the pixel under consideration that contains "pure" information on the surface properties of the pixel.

In (2), atmospheric effects are modeled by atmospheric parameters $\tau_{\mathrm{uw}}(\lambda) \in [0,1], \tau_{\mathrm{dw}}(\lambda) \in [0,1]$ and $L_{\mathrm{a}}(\lambda) \geq 0$. Unfortunately, it is well known that atmospheric correction requires ancillary data (summary statistics), rarely available in practice, which should be collected at several locations within the RS image footprint at the time of RS image acquisition. This means that the problem of atmospheric correction is typically ill- or poorly-posed. Consequently, it is very difficult to solve and requires user's supervision to make it better posed [47]. In practice, this author has observed that RS images radiometrically calibrated into ρ values by several EU institutions mentioned below in this text are affected by spectral distorsion causing scene-derived surface reflectance spectra to disagree with reference surface reflectance spectra found in existing literature (e.g., refer to [64, p. 273]) or in public domain spectral libraries such as the U.S. Geological Survey (USGS) mineral and vegetation spectral libraries, the Johns Hopkins University (JHU) spectral library and the Jet Propulsion Laboratory (JPL) mineral spectral library [47], [65].

A reduction in interscene variability across time, space and sensors can be achieved by a simplification of (2) into dimen-

$$\rho(n,\lambda,t,\mathrm{lat},\mathrm{long}) = \frac{\pi\cdot d(t)^2\cdot\left(\frac{\mathrm{TOARD}(n,\lambda)-L_a(\lambda)}{\tau_{\mathrm{uw}}(\lambda)}\right)}{\mathrm{ESUN}(\lambda)\cdot\cos(\theta_z(t,\mathrm{lat},\mathrm{long}))\cdot\tau_{\mathrm{dw}}(\lambda)+E_d(n,\lambda)} \in [0,1], \quad n = 1,\ldots,N \quad (2)$$

sionless TOARF values belonging to range [0, 1]. Starting from (2), TOARF values are computed as a function of the electromagnetic wavelength for spectral band $b = 1, \ldots, Bnd$, by considering: (a) atmospheric effects negligible, such as for relatively "clear" scenes where $\tau_{\mathrm{uw}}(\lambda) \approx 1, \tau_{\mathrm{dw}}(\lambda) \approx 1$ and $L_{\mathrm{a}}(\lambda) \approx 0$ [42], [45], and (b) flat and/or nonflat neighboring terrain effects negligible, i.e., $E_d(\lambda) \approx 0$ [42]. Thus, (2) becomes [43]

$$\begin{aligned}&\mathrm{TOARF}(n, b, t, \mathrm{lat}, \mathrm{long})\\ &\quad = \frac{\pi \cdot d(t)^2 \cdot \mathrm{TOARD}(n, b)}{\mathrm{ESUN}(b) \cdot \cos(\theta_z(t, \mathrm{lat}, \mathrm{long}))} \in [0, 1]\\ &\qquad\qquad n = 1, \ldots, N, \quad b = 1, \ldots, Bnd. \quad (3)\end{aligned}$$

Although often overlooked by RS scientists and practitioners, it is well known in existing literature that radiometric calibration of DNs into $\mathrm{TOARF} = (3)$ values features several advantages over radiometric calibration into $\mathrm{TOARD} = (1)$ values.

- The former is recommended before calculating various vegetation indices (VIs) [39]. In fact, while the relationships between the leaf area index (LAI) and a great variety of well-known VIs calculated from TOARD values are nonlinear, the relationships between LAI and the same vegetation indices calculated from TOARF are, in several cases, reasonably linear.
- By accounting for seasonal and latitudinal differences in solar illumination the former guarantees better interimage comparability/interpretation (classification, mapping) across time, space and sensors [38], [48], which is in line with the goals of EO data harmonization and interoperability required by the GEOSS and GMES programs.
- The former is more consistent with the scenario of low- and high-level image processing capabilities to be developed on board future intelligent fourth-generation EO satellites (FIEOSs) [49]. According to [50], the increasing need to acquire timely information about Earth system processes and for early warning of natural and human disasters, combined with a need to control costs and cope with increased system complexity, suggests that intelligent satellites are appropriate for deriving information quickly and in near real-time (e.g., value-added products, such as thematic maps, should be generated on board via user commands) for dissemination to nonscience-user communities (e.g., by means of a direct downlink to a mobile device such as a cell phone or laptop computer). To summarize, the development of FIEOS, where on-board integration of sensors, data processors, and communication systems is pursued, should become a major scientific challenge to the RS community within the next 10 years [49].

It is noteworthy that, when neighboring terrain effects are omitted, i.e., $E_d(\lambda) \approx 0$, then $\rho = (2) = \mathrm{f}_1(\mathrm{TOARD})$ can be expressed as $\rho = \mathrm{f}_2(\mathrm{TOARF})$ as follows:

$$\begin{aligned}&\rho(n, \lambda, t, \mathrm{lat}, \mathrm{long}) = (2) \in [0, 1]\\ &\quad \approx \mathrm{TOARF}(n, b, t, \mathrm{lat}, \mathrm{long}) \cdot \frac{1}{\tau_{\mathrm{uw}}(\lambda) \cdot \tau_{\mathrm{dw}}(\lambda)}\\ &\qquad - \frac{\pi \cdot d(t)^2}{ESUN(\lambda) \cdot \cos(\theta_z(t, \mathrm{lat}, \mathrm{long}))}\\ &\qquad \cdot \frac{L_a(\lambda)}{\tau_{\mathrm{uw}}(\lambda) \cdot \tau_{\mathrm{dw}}(\lambda)}\\ &\quad = (3) \cdot \mathrm{AtmphEffct}_1(\lambda)\\ &\qquad - \frac{\pi \cdot d(t)^2}{\mathrm{ESUN}(\lambda) \cdot \cos(\theta_z(t, \mathrm{lat}, \mathrm{long}))}\\ &\qquad \cdot \mathrm{AtmphEffct}_2(\lambda),\\ &\qquad\qquad n = 1, \ldots, N, b = 1, \ldots, Bnd \quad (4)\end{aligned}$$

where $\mathrm{AtmsphEffct}_1(\lambda) = \{1/[\tau_{\mathrm{uw}}(\lambda) \cdot \tau_{\mathrm{dw}}(\lambda)]\} \geq 1$ and $\mathrm{AtmsphEffct}_2(\lambda) = \{L_{\mathrm{a}}(\lambda)/[\tau_{\mathrm{uw}}(\lambda) \cdot \tau_{\mathrm{dw}}(\lambda)]\} \geq L_{\mathrm{a}}(\lambda) \geq 0$. Equation (4) shows that, if flat and non-flat neighboring terrain effects are negligible, i.e., $E_d(\lambda) \approx 0$, then:

- For a clear sky condition, when $\tau_{\mathrm{uw}}(\lambda) \approx 1, \tau_{\mathrm{dw}}(\lambda) \approx 1$ and $\mathrm{L_a}(\lambda) \approx 0$ [42], [45], then $\mathrm{AtmsphEffct}_1(\lambda) \approx 1$ and $\mathrm{AtmsphEffct}_2(\lambda) \approx 0$, thus $\rho = (2) \approx (4) \approx \mathrm{TOARF} = (3)$, i.e., surface reflectance ρ values can be computed from TOARF values when atmospheric effects are: (I) accounted for, i.e., scene-specific parameters $\tau_{\mathrm{uw}}(\lambda), \tau_{\mathrm{dw}}(\lambda)$, and $L_{\mathrm{a}}(\lambda)$ are retrieved from ancillary data, or (II) considered negligible, i.e., surface reflectance ρ values are an ideal (atmospheric noise-free) case of TOARF values. In other words, if $E_d(\lambda) \approx 0$, then $\mathrm{TOARF} = (3) \supseteq \rho = (2) \approx (4)$.
- Independent of wavelength λ, when atmospheric effects are omitted (ignored), i.e., $\mathrm{AtmsphEffct}_1(\lambda) = 1$ and $\mathrm{AtmsphEffct}_2(\lambda) = 0$ such that $\rho = (2) \approx \mathrm{TOARF} = (3)$, numerical effects of the two simplified atmospheric terms, $1 \leq \mathrm{AtmsphEffct}_1(\lambda) = 1$ and $0 \leq L_{\mathrm{a}}(\lambda) \leq \mathrm{AtmsphEffct}_2(\lambda) = 0$, tend to counterbalance each other, i.e., whereas the first approximation causes an underestimation of the ρ estimate, the second approximation does vice versa. Across wavelengths, this property improves the effectiveness of TOARF as an estimator of the true ρ values.
- When wavelength λ increases, TOARF provides a better approximation of ρ. It is well known that light scattering due to atmospheric conditions (haze, consisting of gas molecules and water droplets) and aerosols (consisting of liquid droplets and solid particles suspended in the atmosphere and generated by either natural or anthropogenic sources) is inversely proportional to the energy wavelength λ, i.e., shorter wavelengths of the spectrum are scattered more than the longer wavelengths. Thus, a visible blue (B) channel is affected by scattering across all atmospheric conditions ranging from 'very clear' (where scattering is proportional to a factor λ^{-4}) to 'very hazy' (where scattering is proportional to a factor $\lambda^{-0.5}$) and cloudy (where complete scattering occurs, proportional to a factor λ^0) [45]. On the contrary, in the medium infra-red (MIR) wavelengths the amount of atmospheric scattering is known to be "quite small except for 'very hazy' atmospheres and can be considered negligible" [45, p. 476]. In these various atmospheric conditions, ranging from "very clear" and "clear" visible wavelengths to any MIR portion of the electromagnetic spectrum unless it is "very hazy," atmospheric effects can be omitted (ignored), i.e., $1 \leq \mathrm{AtmsphEffct}_1(\lambda) = 1$ and

$0 \leq L_a(\lambda) \leq \text{AtmsphEffct}_2(\lambda) = 0$ in (4), such that $\rho = (4) = \text{TOARF}$.

B. Operational Automatic RS-IUSs

The goal of this section is to prove that radiometric calibration of RS imagery is a necessary but not sufficient condition for development of operational automatic RS-IUSs. In particular, this section describes advantages and limitations of existing RS-IUS instantiations belonging to the following taxonomy of RS-IUS architectures.

- Multi-agent hybrid RS-IUSs, including the subclass of two-stage stratified hierarchical RS-IUSs.
- Two-stage segment-based RS-IUSs.

1) Multi-Agent Hybrid RS-IUSs: Interaction of intelligent agents in a multi-agent system creates a so-called agent, or cognitive, architecture. If an agent system consists of both symbolic (model-driven, refer to Section I) and sub-symbolic (data-driven, refer to Section I) components capable of mutual (bi-directional) interaction (e.g., if agent A queries agent B then B answers A), then it is called a multi-agent hybrid system [51]. Examples of multi-agent hybrid RS-IUSs found in existing literature are the blackboard model [52], SIGMA [11], ACRONYM [53], SPAM [54], AIDA [55], and ERNEST [56]. Multi-agent hybrid RS-IUSs comprise the following.

i) A low-level general-purpose domain-independent inductive-learning (fine-to-coarse, bottom-up, asemantic, sub-symbolic, refer to Section I) driven-without-knowledge inherently ill-posed image segmentation first stage working at the signal level (data-driven).

ii) A high-level (symbolic) processing second stage combining top-down (model-driven) with bottom-up (data-driven) inference strategies to: (a) better condition an otherwise ill-posed driven-without-knowledge segmentation first stage and (b) restrict intensive processing to a small portion of the image data, analogously to a focus of visual attention in pre-attentive biological vision. Top-down inference is implemented by means of semantic nets representing the application-specific (3-D) scene domain knowledge available *a priori*. A semantic net is defined as a graph, either directed or nonoriented, either cyclic or acyclic, consisting of nodes linked by edges. Nodes represent concepts, i.e., classes of (3-D) objects in the world, while edges represent relations (e.g., PART-OF, A-KIND-OF, spatial relations, temporal transitions) between nodes [104].

Multi-agent hybrid systems typically suffer from two main limitations. First, they are affected by so-called artificial insufficiency caused by the inherent ill-posedness of the image segmentation problem [11]. In practice, any first-stage image segmentation algorithm is simultaneously affected by both omission and commission segmentation errors. Second, semantic nets lack flexibility and scalability to cope with users' changing needs, i.e., they are unsuitable for commercial RS image processing software toolboxes and remain limited to scientific applications.

2) Two-Stage Segment-Based RS-IUSs: Two-stage segment-based RS-IUSs, whose conceptual foundation is known as object-based image analysis (OBIA) [57], have recently gained noteworthy popularity in scientific and commercial VHR image applications where a target land cover class, such as a class of manmade (3-D) objects, can be characterized by salient geometric (morphological, shape) properties and spatial relationships to be computed on a (2-D) image segment basis [6]. Unlike multi-agent hybrid RS-IUSs, a two-stage segment-based RS-IUS architecture comprises an inherently ill-posed driven-without-knowledge segmentation first stage in series with a segment-based classifier unable to interact with the first stage to make it better posed. In particular, see the following.

i) The inherently ill-posed driven-without-knowledge segmentation first stage is: (a) inherently affected by artificial insufficiency, i.e., it is inherently affected by both omission and commission segmentation errors (see comments above in Section III-B1 above) and (b) relies on segmentation parameters to be user-defined based on heuristics. To reduce the number of empirical segmentation parameters, commercial two-stage segment-based RS-IUSs employ a multiscale (hierarchical) iterative segmentation first stage [105]. As output, a hierarchical segmentation algorithm generates multiscale segmentation solutions in the hope that the target image will appear correctly segmented at some scale. Unfortunately, quantitative multiscale assessment of segmentation quality indices requires ground truth data at each scale which are impossible or impractical to obtain in RS common practice. Therefore, the "best" segmentation map must be selected by the user on an *a posteriori* basis from the available set of multiscale segmentation solutions according to heuristic, subjective and/or qualitative criteria analogous to those employed in the selection of prior segmentation parameters [106]. To conclude, exploitation of a hierarchical segmentation algorithm does not make the driven-without-knowledge segmentation first stage easier to use. In addition, hierarchical segmentation algorithms are computationally intensive and require large memory occupation.

ii) A segment-based classification second stage can be implemented either top-down (model-driven), such as a decision-tree classifier based entirely upon prior knowledge of the (3-D) world, or bottom-up (data-driven), such as a supervised data learning classifier. In practice, under the guise of "flexibility" two-stage segment-based RS-IUS software toolboxes provide RS experts and practitioners with overly complicated options to choose from based on heuristics and, as a consequence, they are difficult to use [57]. In addition, the second-stage classifier is unable to interact with the driven-without-knowledge segmentation first stage to make the inherently ill-posed segmentation problem better posed (see Section III-B1 above). Finally, as input information primitives the second stage classifier employs sub-symbolic (2-D) segments exclusively. This may be unnecessary and time-consuming when, for example, simple pixel-based spectral properties can be employed for classification purposes.

Overall, there is still a lack of consensus and research on the conceptual foundation of OBIA, i.e., on the relationship between inherently ill-posed sub-symbolic (2-D) image segments and symbolic (3-D) landscape objects [57].

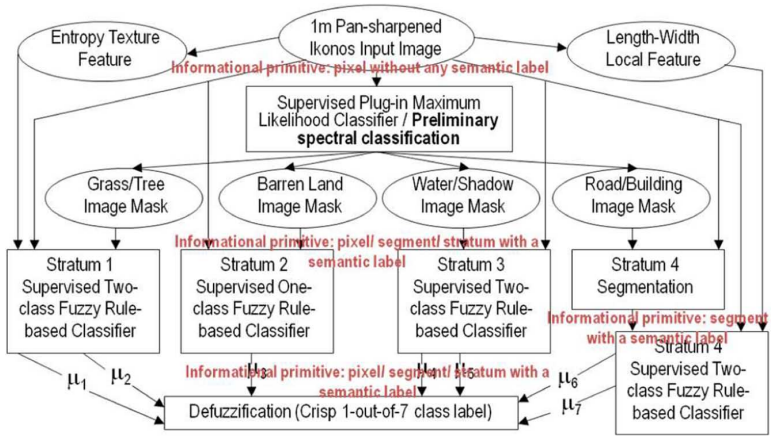

Fig. 1. Two-stage stratified hierarchical RS-IUS implementation proposed by Shackelford and Davis [58], [59]. As output the preliminary classification first stage provides simultaneously: (i) symbolic pixels, (ii) symbolic segments (objects, parcels, as connected sets of labeled pixels featuring the same label), and (iii) symbolic strata (as image-wide sets of labeled pixels featuring the same label). These data types co-exist and are all provided with a semantic meaning which is well understood by a user.

3) Two-Stage Stratified Hierarchical RS-IUSs: In recent years Shackelford and Davis have presented several implementations of a two-stage RS-IUS model suitable for mapping VHR satellite images of urban areas [58], [59]. These RS-IUS implementations comprise, in cascade (see Fig. 1): (i) a supervised pixel-based plug-in (i.e., noniterative, one-pass) maximum likelihood (ML) classifier and (ii) a battery of class-specific classification modules. Starting from the customary distinction between a model and its implementation, this author considers the Shackelford and Davis RS-IUS instantiations the first examples found in RS literature of a novel family of RS-IUSs, called hereafter the two-stage stratified hierarchical RS-IUS model, whose stratification mechanism works analogously to a focus of visual attention in biological vision. This novel RS-IUS architecture constitutes a subclass of the parent class of multi-agent hybrid systems for RS image understanding (see Section III-B1 above) and represents a possible alternative to the ordinary well-known two-stage segment-based RS-IUS model (see Section III-B2 above).

The objective of this section is threefold.

- To summarize the Shackelford and Davis RS-IUS implementations.
- To highlight advantages of the two-stage stratified hierarchical RS-IUS architecture.
- To present an enhanced instantiation of the two-stage stratified hierarchical RS-IUS model whose pixel-based preliminary classification first stage is implemented, in place of the ordinary supervised plug-in ML classifier adopted by Shackelford and Davis, as an operational automatic near real-time well-posed model-driven application-independent spectral rule-based decision-tree classifier (SRC) recently proposed to the RS community [15], [16], [60].

a) Shackelford and Davis RS-IUS Implementation: Suitable for mapping 1 m resolution VHR imagery of urban areas the Shackelford and Davis two-stage RS-IUS implementation comprises, in cascade (see Fig. 1) [58], [59].

i) A pixel-based preliminary classifier implemented as a supervised pixel-based plug-in (noniterative, one-pass) maximum likelihood (ML) classifier that maps each pixel into a discrete and finite set of semantic labels. In place of ordinary land cover classes, these semantic labels identify land cover class sets [58], [59], i.e., they "combine" sets of primitive land cover classes. More specifically, each class set is a logical OR combination of primitive land cover classes affected by ML classification confusion due to a significant amount of spectral overlap. This is tantamount to saying that the ML classification confusion between different class sets is negligible, i.e., land cover class sets must be mutually exclusive. In other words, the first-stage pixel-based plug-in ML classifier implemented by Shackelford and Davis is well posed. Given the structural content of urban scenes depicted in VHR spaceborne imagery, five class sets are identified (see Fig. 1): (1) *either grass or tree*, (2) *either road or building or impervious surface*, (3) *either water or shadow*, (4) *bare soil*, and (5) *others* (outliers, e.g., clouds). In line with the Congalton requirements, this classification scheme is mutually exclusive and totally exhaustive [33, p.12].

ii) A battery of land cover class (object model)-specific (knowledge-driven) hierarchical classifiers incorporating the "stratified" or "layered" approach which is typically adopted in decision-trees [14]. This battery consists of (see Fig. 1): (a) stratified context-sensitive (e.g., texture) feature extraction modules and (b) stratified land cover class-specific fuzzy rule-based classification modules employing a converge-of-evidence mechanism.

b) Advantages of the Two-Stage Stratified Hierarchical RS-IUS Architecture: In comparison with the parent class of multi-agent hybrid RS-IUSs (see Section III-B1 above) the subset class of two-stage stratified hierarchical RS-IUSs features one major advantage. While primitive (2-D) objects employed by the former are sub-symbolic (asemantic) segments (e.g., segment 1, segment 2, etc.) the latter employs primitive (2-D) objects comprising symbolic pixels in symbolic segments in symbolic strata. In practice, by providing RS application developers and domain experts with semantic (symbolic) primitive (2-D) objects in the image domain, the two-stage stratified

hierarchical RS-IUS architecture facilitates instantiation of multi-agent hybrid systems for RS image understanding [15].

In comparison with the two-stage segment-based RS-IUS architecture (refer to Section III-B2) the two-stage stratified hierarchical RS-IUS model features several potential advantages which are listed below [15].

1. A pixel-based preliminary classification first stage features several advantages over a first-stage driven-without-knowledge segmentation algorithm.
   - — The former is not affected by the well-known *uncertainty principle* according to which, for any contextual (neighborhood) property, we cannot simultaneously measure that property while obtaining accurate localization [107]. In other words, by working at the sensor spatial resolution the pixel-based preliminary classification first stage offers a capability of detecting small but genuine image details potentially superior (at least not inferior) to any context-sensitive segmentation algorithm. In addition, by working at the sensor resolution the former is spatial resolution-independent.
   - — As output a pixel-based preliminary classifier identifies mutually exclusive class sets, called hereafter *spectral-based semi-concepts* which, by definition, are affected by no spectral overlap (refer to this text above). This is tantamount to saying that a pixel-based preliminary classifier is *well posed* and capable of removing any source of artificial insufficiency (uncertainty, unreliability) of sub-symbolic image features traditionally introduced by a first-stage ill-posed driven-without-knowledge segmentation algorithm. A *spectral-based semi-concept is a semantic conjecture based solely on per-pixel (noncontextual) color (spectral, i.e., chromatic and achromatic) properties*. For example, if the "color" (spectral signature) of a pixel is, say, green in the visible electromagnetic spectrum, then that pixel is likely to belong to a spectral-based semi-concept called vegetation whose information granularity is equal to or coarser than that of primative land cover classes (concepts in the [3-D] world) such as, say, *forest* or *grassland*. In practice, *spectral-based semi-concepts are suitable for filling in the well-known information gap between concepts in the (3-D) scene and sub-symbolic features in the (2-D) image* (refer to Section I). Since spectral-based semi-concepts are affected by no spectral overlap, they are reliable and eligible for splitting into their primitive land cover classes at a further hierarchical RS data processing level where sources of contextual evidence (e.g., textural, morphological, geometric properties, spatial relationships, etc.) are taken into consideration.
   - — While driven-without-knowledge segmentation provides ill-posed image segments as sub-symbolic primitive (2-D) objects, a pixel-based preliminary classification first stage generates as output symbolic primitive (2-D) objects comprising symbolic pixels in symbolic segments in symbolic strata. These three spatial types are not alternative, but co-exist and can be selected at second stage according to the needs of the battery of application-specific satellite-based measurement systems.
2. In series with the preliminary image classification first stage, a battery of second-stage stratified class-specific hierarchical classification modules enforces a well-known divide-and-conquer problem-solving approach traditionally employed by decision-tree classifiers [14]. The idea of stratification is well known in statistics. For example, in stratified sampling the sampling frame is divided into nonoverlapping groups or strata, e.g., geographical areas. A sample is taken from each stratum and when this sample is a simple random sample the method is referred to as stratified random sampling. A possible disadvantage is that identification of appropriate strata may be difficult. The advantage is that *stratification will always achieve greater precision provided that the strata have been chosen so that members of the same stratum are as similar as possible with respect to the characteristic of interest*. The second-stage battery of stratified class-specific hierarchical classification modules consists of (see Fig. 1) the following.
   a) Stratified class-specific context-sensitive (e.g., texture, morphological, geometric) feature extraction modules. For example, the "stratified" or "layered" approach is adopted to make an inherently ill-posed segmentation algorithm better posed (locationally constrained). In particular, a second-stage class-specific stratified segmentation algorithm can be employed when a target land cover class is characterized by salient geometric (morphological, shape) properties to be computed as segment-based. This is typically the case of manmade objects, such as buildings, roads and agricultural fields, whose geometric attributes are especially important for their recognition (see Fig. 1).
   b) Stratified class-specific fuzzy rule-based classification modules employing constructive reasoning. In practice, constructive reasoning is pursued through evidence accumulation (convergence-of-evidence) by means of fuzzy membership functions (e.g., elongation is high) and fuzzy operators [58], [59]. It is noteworthy that if-then rules combining symbolic and sub-symbolic sources of evidence can be, firstly, easily modeled by a human domain-expert who is naturally acquainted with symbolic reasoning and, secondly, implemented seamlessly in a two-stage stratified hierarchical RS-IUS architecture where symbolic (2-D) primitives are provided as output by the preliminary classification first stage.
3. In a two-stage stratified hierarchical RS-IUS architecture, the *world model* is twofold.
   - — A first-stage world model is stored in the pixel-based preliminary classifier. It consists of spectral-based semi-concepts described by terms of the terminology defined in the real-world (e.g., either water or shadow, vegetation, etc.).
   - — A second-stage world model consists of semantic nets whose nodes ([3-D] object-models) incorporate the

"stratified" or "layered" approach. This means that in addition to the 3-D appearance properties (e.g., the length of a ship is between 3 and 300 m), an object model comprises, among its attributes, a list of color-based semi-concepts equivalent to a model-specific locational constraint (focus of attention by stratification, e.g., the spectral signature of a ship does not belong to the set of spectral categories cloud, vegetation, water and snow automatically detected in the preliminary classification first stage).

These considerations imply that the degree of prior knowledge embedded in the two-stage stratified hierarchical RS-IUS model and required to complement the intrinsic insufficiency of image features (refer to Section I above) is superior to that adopted by the two-stage segment-based RS-IUS architecture (see Section III-B2 above). As a consequence, the former RS-IUS architecture is eligible for finding a better solution to the ill-posed image-understanding problem than the latter.

c) Enhanced Two-Stage Stratified Hierarchical RS-IUS Implementation: The main drawback of the two-stage stratified hierarchical RS-IUS implementation proposed by Shackelford and Davis is its need for supervised training data at every hierarchical stage [58], [59]. Unfortunately, the costs, quality and availability of adequate training labeled (reference) samples are the most limiting factor for the application of scene-by-scene inductive supervised data learning algorithms (e.g., artificial neural networks [12]) to RS data understanding problems across time, space and sensors (refer to Section II above) [1].

To reduce to zero the need for supervised training data of the plug-in ML classifier implemented by Shackelford and Davis as the preliminary spectral classification first stage, the fully automated SRC system of systems can be adopted instead, refer to Section III-B4 below.

4) Operational Automatic SRC System of Systems: In line with the visionary goal of a GEOSS promoted by GEO, SRC identifies an integrated system of systems comprising: (i) an original Landsat-like SRC (LSRC), capable of mapping radiometrically calibrated 7-band Landsat-like images generated from spaceborne optical sensors such as the Landsat-5 Thematic Mapper (TM), the Landsat-7 Enhanced TM (ETM)+, the Advanced Spaceborne Thermal Emission and Reflection Radiometer (ASTER) and the Moderate Resolution Imaging Spectroradiometer (MODIS) [60], and (ii) several down-scaled versions of LSRC, suitable for mapping multispectral (MS) images acquired by almost any of the existing or future planned satellite optical imaging sensors whose spectral resolution overlaps with, but is inferior to Landsat's [15], refer to Tables I and II. The down-scaled LSRC versions are generated by removing the excess spectral channels from the 7-band LSRC rule set while enforcing equivalences between the remaining (E)TM bands and the sensor bands at hand [15], refer to Table II.

The degree of novelty of SRC is fourfold [15], [16], [60].

1. The integrated SRC system of systems *requires neither user-defined parameters nor reference data samples to run upon input MS imagery acquired across time, space and sensors*, see Figs. 2–11. Therefore, SRC is termed "fully automated" [103]. To the best of this author's knowledge, no multisource, multiresolution fully automated optical image mapping system alternative to SRC does exist in literature.
2. SRC is a one-pass (noniterative) decision-tree classifier not adaptive to data, i.e., SRC is model-based (refer to Section I above) where (3-D) object-models of the real (3-D) world rely upon prior spectral knowledge exclusively. In particular, the SRC prior spectral knowledge consists of decision rules generated from endmember collection spectra extracted from a wide variety of real-world MS satellite images radiometrically calibrated into TOARF values, with $\mathrm{TOARF} = (3) \supseteq \rho = (2)$, rather than surface reflectance ρ values adopted exclusively by competing approaches such as [47]. It is noteworthy that, if $E_d(\lambda) \approx 0$ then, according to (4), when atmospheric effects are removed or considered negligible, the reference dictionary of endmember spectra in TOARF values employed by SRC coincide with ground measured or library surface reflectance spectra [47], [65]. In other words, ground measured or library surface reflectance spectra are a subset of the parent class of endmember collection spectra in TOARF values adopted by SRC. This is tantamount to saying that the only SRC requirement is to employ as input a well-behaved *MS image transformed into either* $\mathrm{TOARF} = (3)$ *or* $\rho = (2)$ *values, the latter being an ideal case of the former when atmospheric effects are removed or considered negligible* (refer to Section III-A above). As a consequence, SRC may benefit from but requires no inherently ill-posed atmospheric correction preprocessing stage. In other words, SRC considers atmospheric correction an optional MS image preprocessing stage unlike competing classification approaches employing surface reflectance spectra, such as ATCOR3 [47], for which solution of the ill-posed atmospheric correction problem becomes mandatory. At best (when no spectral distorsion is introduced, refer to Section III-A above), a mandatory atmospheric correction stage decreases the overall operational performance measurement of a data product generation and delivery chain (due to a decrease in the degree of automation, an increase of costs required to gather ancillary data and an overall increase of timeliness, refer to Section II).

TABLE I
TABLE OF ACRONYMS

Portion of the electromagnetic spectrum	Adopted acronyms	Wavelengths, if any (μm).
Multi-spectral	MS	
Panchromatic	PAN	
Violet	V	0.35-0.45
Blue	B	0.45-0.50
Green	G	0.50-0.57
Yellow	Y	0.57-0.60
Orange	O	0.60-0.65
Red	R	0.65-0.72
Near Infra-Red	NIR	0.72-1.3
Middle IR	MIR	1.3-3.0
Far IR	FIR	7.0-15.0
Thermal IR	TIR	8.0-12.0

TABLE II
SATELLITE OPTICAL SENSORS: TECHNICAL CHARACTERISTICS

	Mission date	PAN (μm)	Spatial Resol. PAN (m)	MS (μm)	Spatial Resol. MS (m)	Bits	Revisit Time, depen-ding on latitude (days)	Swath Width (km)	Full Scene Cove-rage Area (km)	Reference
GeoEye-1	Sept. 2008 to present	0.450-0.900	0.41 resam-pled to 0.50 m for non-US Gover-nment custo-mers	1-B: 0.450-0.520, 2-G: 0.520-0.600, 3-R: 0.625-0.695, 4-NIR: 0.760-0.900	1.64	11	< 3	15.2	15×15	http://www.geoanalytic.com/satellite-images/geoeye-1, http://launch.geoeye.com/LaunchSite/assets/documents/geoeye1_factsheet_v9.pdf
IKONOS-2	Sept. 1999 to present	0.450-0.900	1	(a) 1-B: 0.445-0.516, 2-G: 0.506-0.595, 3-R: 0.632-0.698, 4-NIR: 0.757-0.853 (b) 1-B: 0.45-0.52, 2-G: 0.52-0.60, 3-R: 0.63-0.69, 4-NIR: 0.76-0.80 (c) 1-B: 0.450-0.520, 2-G: 0.510-0.600, 3-R: 0.630-0.700, 4-NIR: 0.760-0.850	4	11	3-1.5	11.3	-	(a) http://en.wikipedia.org/wiki/IKONOS, (b) http://www.geog.ucsb.edu/~jeff/115a/history/ikonos.html, http://www.orbimage.com, http://www.geoeye.com, (c) http://amelia.db.erau.edu/nasacds/200606Disc1/research/20060019230_2006011209.pdf
OrbView-3	June 2003 to present	0.450-0.900	1	1-B: 0.450-0.520, 2-G: 0.520-0.600, 3-R: 0.625-0.695, 4-NIR: 0.760-0.900	4		< 3 days	8	User - defined	http://www.orbimage.com, http://www.geoeye.com, http://amelia.db.erau.edu/nasacds/200606Disc1/research/20060019230_2006011209.pdf
QuickBird-2	Oct. 2001 to present	0.450-0.900	0.61	(a) 1-B: 0.450-0.520 , 2-G: 0.520-0.600, 3-R: 0.630-0.690, 4-NIR: 0.760-0.900 (b) 1-B: 0.445-0.510 , 2-G: 0.500-0.595, 3-R: 0.620-0.690, 4-NIR: 0.755-0.875	2.44		1 to 3.5	16.5	-	(a) CD Telespazio and Telespazio QuickBird Listino Prezzi (b) http://amelia.db.erau.edu/nasacds/200606Disc1/research/20060019230_2006011209.pdf
FORMOsa SATellite (FORMOSAT)-2	April 14, 2006	0.45-0.90	2	1-B: 0.45-0.52, 2-G: 0.52-0.60, 3-R: 0.63-0.69, 4-NIR: 0.76-0.90	8	-	1	24×24	-	http://www.spotimage.fr/web/en/977--formosat-2-images.php
KOrean MultiPurpose SATellite (KOMPSAT)-2	July 28, 2006	0.50-0.90	1	1-B: 0.45-0.52, 2-G: 0.52-0.60, 3-R: 0.63-0.69, 4-NIR: 0.76-0.90	4	10 (acquisition), 16 (delivery)	3 to 28	15×15	-	http://www.spotimage.fr/web/en/1155-kompsat-2-images.php
Pleiades-1/-2 (two satellite constellation) High Resolution (HR)	To be launched in 2009 (Pleiades-HR1) and 2009 (Pleiades-HR2)	0.48-0.83	0.60 (at nadir)	1-B: 0.43-0.55, 2-G: 0.49-0.61, 3-R: 0.60-0.72, 4-NIR: 0.75-0.95.	2.8 (at nadir)	16	1 satellite - viewing angle 5°: 26 days, 20°: 7 days, 30°: 5 days; 2 satellites - viewing angle 5°: 13 days, 20°: 5 days, 30°: 2 days.	20	20×20	SPOT_Image_presentation_JRC_June2008.ppt, http://www.sovzond.ru/en/satellites/france/773.html
SPOT-6/-7 AstroTerra program	To be launched in 2012 (SPOT-6) and 2017 (SPOT-7)	0.48-0.83??	2	1-B: 0.43-0.55???, 2-G: 0.49-0.61???, 3-R: 0.60-0.72???, 4-NIR: 0.75-0.95?.	8	8??	2 to 3 (repeat cycle: 26days)	60	60×60	SPOT_6_7_.ppt, JRC, June 2008.
RapidEye (5 satellite constellation)	Sept. 6, 2008 to present	-	-	1-B: 0.440-0.510, 2-G: 0.520-0.590, 3-R: 0.630-0.685, 4-Red Edge: 0.690-0.730,	5	12	1	78	-	http://www.rapideye.de/

3. SRC automatically detects as output spectral-based semi-concepts which, by definition, are affected by no spectral overlap (refer to Section III-B3). *While land cover classes are provided with a superior semantic meaning, but are difficult to detect automatically, spectral-based semi-concepts, which are provided with an inferior semantic meaning, are detected automatically by* SRC [15], [60]. For example, LSRC maps a pixel-based 7-band Landsat-like MS data vector onto a discrete and finite set of forty-six spectral categories belonging to six parent spectral categories (supercategories), which are listed below (according to their order of detection): i) *cloud*, ii) *either snow or ice*, iii) *either water or shadow*, iv) *vegetation*, v) *either bare soil or built-up* and vi) *outliers* [15].
4. *In terms of operational performance* SRC *scored high* when it was subject to independent scientific scrutiny for

TABLE II
(CONTINUED.) SATELLITE OPTICAL SENSORS: TECHNICAL CHARACTERISTICS

				5-NIR: 0.760-0.850						
Advanced Land Observing Satellite (ALOS) Advance Visible and Near Infrared Radiometer type 2 (AVNIR-2)	Jan. 24, 2006 to present	-	-	1-B: 0.42-0.50 , 2-G: 0.52-0.60, 3-R: 0.61-0.69, 4-NIR: 0.76-0.89	10 (at nadir)	8	46	70 (at nadir)	-	http://www.eorc.jaxa.jp/ALOS/about/avnir2.htm
Satellite Pour l'Observation de la Terre (SPOT) -4 HRVIR (High Resolution Visible & Infrared)	March 1998 to present	0.61-0.68	10	1-G: 0.50-0.59, 2-R: 0.61-0.68, 3-NIR: 0.78-0.89, 4-MIR: 1.58-1.75	20	8	2 to 3 (repeat cycle: 26days)	60	60×60	www.spotimage.fr, http://telsat.belspo.be/bEO/en/satellites/spot.htm
SPOT-5 HRG (High Resolution Geometric)	May 2002 to present	0.48-0.71	2.5 (supermode) – 5 (standard pan)	1-G: 0.50-0.59, 2-R: 0.61-0.68, 3-NIR: 0.78-0.89, 4-MIR: 1.58-1.75	10 (G – NIR), 20 (MIR)	8	2 to 3 (repeat cycle: 26days)	60	60×60	www.spotimage.fr, http://telsat.belspo.be/bEO/en/satellites/spot.htm http://ccrs.nrcan.gc.ca/resource/tutor/fundam/chapter2/12_e.php
SPOT-4 and -5 – VMI (Vegetation Monitoring Instrument 1 and 2, respectively)	March 1998 to present			1-B: 0.43-0.47, 2- R: 0.61-0.68, 3-NIR: 0.78-0.89, 4-MIR: 1.58-1.75	1165 (1.1 km)	8	daily	2250	-	www.spotimage.fr, http://www.sebal.us/, http://telsat.belspo.be/bEO/en/satellites/spot.htm
SPOT-1, -2 and -3 HRV (High Resolution Visible)	SPOT-1: Feb. 1986 to Dec. 1990, SPOT-2: Jan. 1990 to present, SPOT-3: Sept. 1993 to Nov. 1997.	0.50-0.73	10	1-G: 0.50-0.59, 2-R: 0.61-0.68, 3-NIR: 0.78-0.89	20	8	2 to 3 (repeat cycle: 26days)	60	60×60	www.spotimage.fr, http://telsat.belspo.be/bEO/en/satellites/spot.htm
Indian Remote sensing Satellite (IRS)-1C/1D, high resolution Linear Imaging Self-Scanner (LISS-IV, PAN camera), medium resolution Linear Imaging Self-Scanner (LISS-III), low resolution Wide Field Sensor (WiFS)	Dec. 1995/Sept. 1997 to present	LISS-IV: 0.50-0.75	5.8 (at nadir) -10	LISS-III, 1-G (B2): 0.52-0.59, 2-R (B3): 0.62-0.68, 3-NIR (B4): 0.77-0.86, 4-MIR (B5): 1.55-1.70 WiFS, 1-R (B3): 0.62-0.68, 2-NIR (B4): 0.77-0.86	LISS-III: 23.5 (G – NIR), 70 (MIR), WiFS: 188	7	24	LISS-IV, PAN: 70, LISS-III: 127-141, WiFS: 720	LISS-IV:70×70, LISS-III: 140×140, WiFS: 720×720	CD_eurimage , http ://ccrs.nrcan.gc.ca/resource/tutor/fundam/chapter2/12_e.php http ://directory.eoportal.org/pres_IRS1C1D.html, http://earth.esa.int/pub/ESA_DOC/IRSP6/HANDBOOK_Resourceat-1_IRS-P6.pdf
IRS-P6 (Resourcesat-1) High resolution Linear Imaging Self-Scanner (LISS-IV), medium resolution Linear Imaging Self-Scanner (LISS-III), low resolution Advanced Wide Field Sensor (AwiFS)	Oct. 2003 to present.	-	-	LISS-IV, 1-G (B2) : 0.52-0.59, 2-R (B3) : 0.62-0.68, 3-NIR (B4) : 0.77-0.86. LISS-III, 1-G (B2): 0.52-0.59, 2-R (B3): 0.62-0.68, 3-NIR (B4): 0.77-0.86, 4-MIR (B5): 1.55-1.70 AwiFS = LISS-III	LISS-IV: 5.8, LISS-III: 23.5, AwiFS: 56	LISS-III and LISS-IV: 7, AwiFS: 10	LISS-III: 24, LISS-IV and AwiFS (due to steerability): 5	LISS-IV, MONO mode (B3) : 70.3, MX mode (B2, B3, B4) : 23.5, LISS-III : 141, AwiFS : 720		http://www.isro.org/pslvc5/index.html http ://directory.eoportal.org/info_IRSP6IndianRemoteSensingSatellite.html, http://earth.esa.int/pub/ESA_DOC/IRSP6/HANDBOOK_Resourceat-1_IRS-P6.pdf
Landsat 5 TM (Thematic Mapper)	March 1, 1984 to present?			1-B: 0.45-0.52, 2-G: 0.52-0.60, 3-R: 0.63-0.69, 4-NIR: 0.76-0.90,	Bands 1-5, 7: 30, Band 6: 120.	8	16	185	172.8×185	CD_Eurimage

validation over a wide range of spatial conditions, time periods, geographic extents and optical imaging sensors [15], [16]. SRC was considered: (a) fully automated (see this text above), (b) accurate, (c) near real-time (e.g., it requires approximately 5 minutes to process a Landsat scene on a desktop computer provided with a Dual Core Pentium pro-

TABLE II
(*CONTINUED.*) SATELLITE OPTICAL SENSORS: TECHNICAL CHARACTERISTICS

				5-MIR1: 1.55-1.75, 6-TIR: 10.4-12.5, 7-MIR2: 2.08-2.35						
Landsat 7 ETM+ (Enhanced Thematic Mapper)	April 15, 1999 to April 2003	0.52-0.90	15	1-B: 0.45-0.52, 2-G: 0.52-0.60, 3-R: 0.63-0.69, 4-NIR: 0.76-0.90, 5-MIR1: 1.55-1.75, 6-TIR: 10.4-12.5, 7-MIR2: 2.08-2.35	Bands 1-5, 7: 30, Band 6: 60.	8	16	185	172.8×185	CD_Eurimage
CBERS-1 and -2 (China-Brazil Earth Resources Satellite) - subsystems CCD camera: band 1-4, InfraRed Multi-Spectral Scanner (IRMSS) : band 5-7.	October 14, 1999 and Oct 21, 2003, respectively, to present	CCD-0.51-0.73, IRMSS-0.50-1.10	CCD-20, IRMSS-80.	1-B: 0.45-0.52, 2-G: 0.52-0.59, 3-R: 0.63-0.69, 4-NIR: 0.77-0.89, 5-MIR1: 1.55-1.75, 6-MIR2: 2.08-2.35, 7-TIR: 10.40-12.50.	Bands 1-4: 20, Bands 5-6: 80, Band 7: 160.		26	CCD-113, IRMSS-120	CCD-113×113, IRMSS-120×120 CCD-113, IRMSS-120 CCD-113, IRMSS-120 CCD-113, IRMSS-120	http://www.cbers.inpe.br/en/index_en.htm
ASTER (Advanced Spaceborne Thermal Emission and Reflection Radiometer)– subsystems Very Near IR (VNIR): band 1-3, Short Wave IR (SWIR) : band 4-9, and Thermal IR (TIR): band 10-14.	Dec. 18, 1999 to present			1-G: 0.52-0.60. 2-R: 0.63-0.69. 3-NIR: 0.76-0.86. 4-MIR1: 1.600-1.700. 5-MIR2: 2.145-2.185. 6-MIR3: 2.185-2.225. 7-MIR4: 2.235-2.285. 8-MIR5: 2.295-2.365. 9-MIR6: 2.360-2.430. 10-TIR1: 8.125-8.475. 11-TIR2 : 8.475-8.825. 12-TIR3 : 8.925-9.275. 13-TIR4 : 10.25-10.95. 14-TIR5 : 10.95-11.65.	Bands 1-3: 15, Bands 4-9: 30, Bands 10-14: 90.	8, but 11 for TIR channels	Daily	60	60×60	http://edcdaac.usgs.gov/aster, http://www.sebal.us/ http://aster.indomicrowave.com/bandspectrum.htm
Disaster Monitoring Constellation (DMC) consisting of the Alsat-1, Deimos-1, Beijing-1, UK-DMC, UK-DMC2 and Nigeria Sat-1 SLIM6 instrument	2002 (Alsat-1) to 2008 (UK-DMC2)	?	4 (Beijing-1)	1-G: 0.52 - 0.60 2-R: 0.63 - 0.69 3-NIR: 0.77 - 0.90	Deimos-1, UK-DMC2: 22, all others: 32.	?	1 (MS) to 5 (PAN)	660	660 × 4,100 (MS)	http://www.dmcii.com/
MODIS (Moderate Resolution Imaging Spectroradiometer), TERRA (EOS AM) and AQUA (EOS PM) satellites **NOTE: data format MOD021KM: all 36 bands, 1 km res. Data format MOD02QKM: bands 1 and 2, 250 m res. Data format MOD02HKM, bands 1 to 7, 500 m resolution.**	Terra: Dec. 18, 1999 to present. Aqua: May 4, 2002, to present.			1-O/R1: 0.620 – 0.670 2-NIR1: 0.841 – 0.876 3-B1: 0.459 – 0.479 4-G1: 0.545 – 0.565 5-NIR2: 1.230 – 1.250 6-MIR1: 1.628 – 1.652 7-MIR2: 2.105 – 2.155 8-V1: 0.405 – 0.420 9-V2: 0.438 – 0.448 10-B2: 0.483 – 0.493 11-G2: 0.526 – 0.536 12-G3 : 0.546 – 0.556 13-R2 : 0.662 – 0.672 14-R3 : 0.673 – 0.683 15-NIR3: 0.743 – 0.753 16-NIR4: 0.862 – 0.877 17-NIR5: 0.890 – 0.920 18-NIR6: 0.931 – 0.941 19-NIR7: 0.915 – 0.965 20-MIR3: 3.660 – 3.840 21-MIR4: 3.929 – 3.989 22-MIR5: 3.929 – 3.989 23-MIR6: 4.020 – 4.080	Bands 1-2: 250, Bands 3-7: 500, Bands 8-36: 1000 (1 km).	12	One to two days	2330	2330×10	http://modis.gsfc.nasa.gov/about/specifications.php

cessor), (d) robust to changes in the input image acquired across time, space and sensors, (e) capable of providing a preliminary classification map whose semantic granularity is much finer than that provided by the ML first stage of the Shackelford and Davis RS-IUS implementations and (d) not affected by the well known salt-and-pepper clas-

TABLE II
(CONTINUED.) SATELLITE OPTICAL SENSORS: TECHNICAL CHARACTERISTICS

				24-MIR7: 4.433 – 4.498 25-MIR8: 4.482 – 4.549 26-MIR9: 1.360 – 1.390 27-MIR10: 6.535 – 6.895 28-FIR1: 7.175 – 7.475 29-TIR1: 8.400 – 8.700 30-TIR2: 9.580 – 9.880 31-TIR3: 10.780 – 11.280 32-TIR4: 11.770 – 12.270 33-FIR2: 13.185 – 13.485 34-FIR3: 13.485 – 13.785 35-FIR4: 13.785 – 14.085 36-FIR5: 14.085 – 14.385						
NOAA (National Oceanic and Atmospheric Administration) AVHRR (Advanced Very High Resolution Radiometer), Satellite numbers 15 to 17	Oct. 1978 to present			1-Y/O/R: 0.58-0.68, 2- NIR: 0.725-1.10, 3 [3(A)]-MIR1(in Satellite no. 15, 16, and 17, exclusively, acquired day-time): 1.58-1.64, 4 [3(B)]-MIR2 (acquired night-time in Satellite no. 15, 16, and17): 3.55-3.93, 5 [14]-TIR1: 10.30-11.30, 6 [13]-TIR2: 11.50-12.50	1100 (1.1 km)		Six daytime passes	2399	-	http://edc.usgs.gov/guides/avhrr.html#avhrr2, http://edc.usgs.gov/guides/avhrr.html#avhrr8
METEOSAT 2nd Generation (MSG) SEVIRI (Spinning Enhanced Visible and IR Imager)	End of 2005 to present			1-Y/O: 0.6 2-NIR: 0.8 3-MIR1: 1.6 4-MIR2: 6.2 5-FIR1: 7.3 6-MIR3: 3.9 7-TIR1: 8.7 8-TIR2: 10.8 9-TIR3: 12.0 10-TIR4: 9.7 11-FIR2: 13.4	Bands 1-3: 1000 (1 km), Bands 4-11: 3000 (3 km).		15 min	-	-	http://www.eumetsat.int/home/Main/Publications/Technical_and_Scientific_Documentation/index.htm?l=en
ENVISAT AATSR (Advanced Along-Track Scanning Radiometer)	March 2002 to present	-	-	1-G: 0.545-0.565, 2-R: 0.649-0.669, 3-NIR: 0.855-0.875, 4-MIR1 (SWIR): 1.46-1.76, 5-MIR2 (MWIR): 3.55-3.85, 6-TIR: 10.35-11.35, 7-TIR: 11.50-12.50	1000 (1 km), at nadir.		3-, 35-(nominal orbit), and 168-day repeat cycles (in the 3-day repeat cycle, AATSR does not achieve full coverage of the Earth)	500	900×512	http://envisat.esa.int/instruments/aatsr/
ENVISAT MERIS (Medium Resolution Imaging Spectrometer Instrument)	March 2002 to present	-	-	Fifteen (15) spectral bands can be selected by ground command, each of which has a programmable width and a programmable location in the 390 nm (VIS) to 1040 nm (NIR) spectral range.	≈ 300 (260 m × 290 m ground resolution), at nadir.	-	3-, 35-(nominal orbit), and 168-day repeat cycles (in all these three repeat cycle, MERIS achieves full coverage of the Earth)	≈ 600 (Full Res., FR), ≈ 1150, (Reduced Res., RR)	582 × 650 (Full Res., FR), ≈ 1150 × 1165, (Reduced Res., RR)	http://envisat.esa.int/handbooks/meris/

sification noise effect which traditionally affects ordinary pixel-based classifiers, i.e., SRC is successful in modelling the within-stratum variance, see Figs. 2–11. These functional attributes make SRC eligible for use as the preliminary pixel-based classification first stage in a two-stage stratified hierarchical RS-IUS architecture [15], [16]. This means that *in a two-stage stratified hierarchical RS-IUS instantiation* (see Fig. 1) *employing* SRC *as its pixel-based preliminary classification first stage, second-stage traditional algorithms capable of learning from either unlabeled or labeled data*, such as unlabeled data clustering and image segmentation algorithms, *which incorporate the "stratified" or "layered" approach are expected to perform better than or the same as their traditional nonstratified counterparts*. This is tantamount to saying that *an operational automatic* SRC *system is preliminary and by no means alternative to traditional algorithms capable of learning from either unlabeled or labeled data which can be enhanced by incorporating the "stratified" or "layered" approach*.

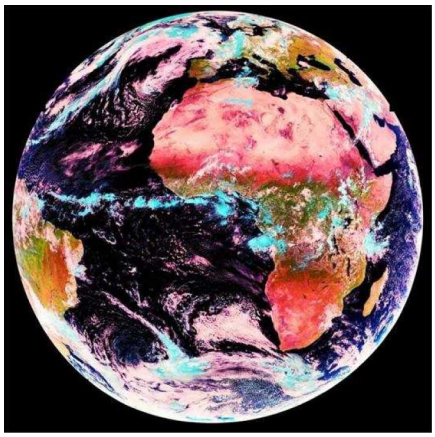

(a)

(b)

Fig. 2. (a) Meteosat Second Generation (MSG) image (acquisition date: 2007-05-16, 12:30) in TOARF values, depicted in false colors (R: band 3, G: band 2, B: band 1). Spatial resolution: 1 km. (b) SRC output map, depicted in pseudo colors. Water and shadow areas are in different shades of blue, clouds in different shades of white, (thin) clouds over water, snow and ice in different shades of light blue, vegetation types in different shades of green, (thin) clouds over vegetation and rangeland types in different shades of light green, barren land types in different shades of brown and grey, unknown pixels (outliers), if any, are shown in red.

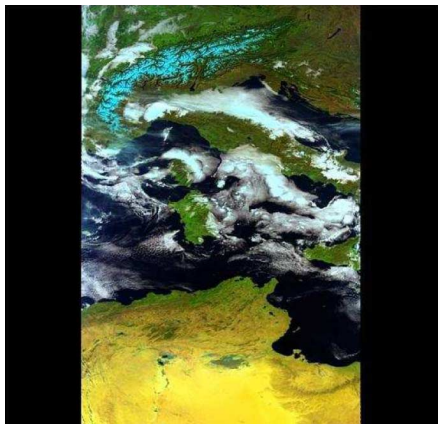

(a)

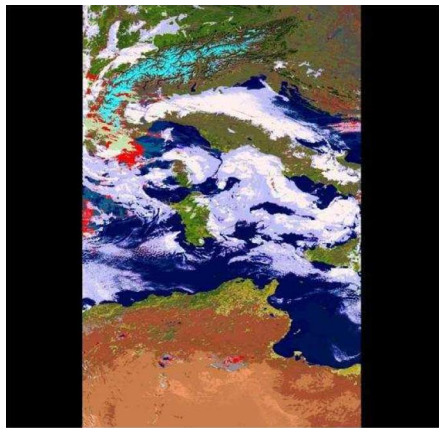

(b)

Fig. 3. (a) MODIS image in TOARF values, acquired on January 5, 2007, covering northern Africa and Italy, depicted in false colors (R: band 1, G: band 4, B: band 3), spatial resolution: 500 m. (b) Output map, depicted in pseudo colors [same as in Fig. 2(b)], automatically generated by SRC from the image shown in Fig. 3(a).

IV. Absolute Radiometric Calibration Zero-Value Offset Parameters in SPOT and IRS Imagery

This section is meant to do the following.

1. Underline that absolute radiometric calibration offset (bias) parameters to be retrieved from the SPOT and IRS metadata files appear to be constant with time and always equal to zero. To date, these observations are ignored or considered irrelevant by the majority of the RS community.
2. Investigate the calibration quality and uncertainty of the SPOT and IRS satellite sensor series in agreement with the QA4EO initiative, despite these issues have been rarely the subject of scientific inquiry by the RS community. For example, the radiometric calibration uncertainty of the Landsat TOARD values is known to be between 5% and 10% [67]. Unfortunately, in existing literature this author was unable to find any radiometric quality and uncertainty estimate holding for the SPOT and IRS sensor series [101].

To the best of this author's knowledge, the SPOT metadata DIMAP file provides offset parameters $B(b), b = 1, \ldots, Bnd$, to be employed in (1), which appear to be constant with time and equal to zero. This is acknowledged by SPOT Image in a personal communication [63] and, to some respect, by existing literature. For example, in [47], Richter writes that in the SPOT metadata files "the standard offset values are zero". In [40], which specifically deals with the SPOT-4 VEGETATION and High Resolution Visible & Infrared (HRVIR) onboard calibration systems and vicarious calibration methods over test sites, the offset calibration term $B(b)$ is omitted from (1). This means that, in the words of an anonymous referee, the SPOT DNs "are assumed to be already equalized and corrected by a dark-object current". If so, a $B(b)$ "offset parameter is used only if, after the DN equalization step, a dynamic adaptation is required". If no dynamic adaptation is applied, then $B(b) = 0$, which appears to be always the case. Actually, this referee's explanation is not supported by the text in [40] where keywords such as "offset," "dark (object)," and "black (object)" are missing.

Based on this author's experience, zero-value offset parameters are always retrieved from the IRS metadata files too. In

(a)

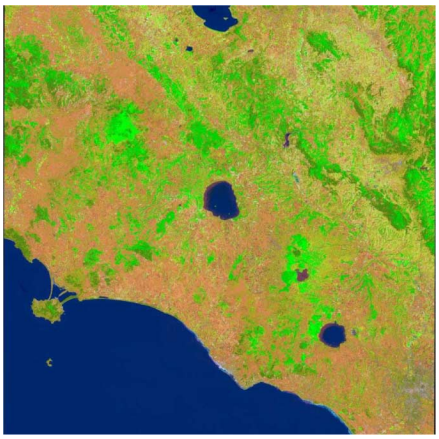

(b)

Fig. 4. (a) IRS-P6 LISS-III image in TOARF values, acquired on July 12, 2006, at 11:52 (CEST), covering Central Italy, depicted in false colors (R: band 4, G: band 3, B: band 1), spatial resolution: 23.5 m. (b) Output map, depicted in pseudo colors [same as in Fig. 2(b)], automatically generated by SRC from the image shown in Fig. 4(a).

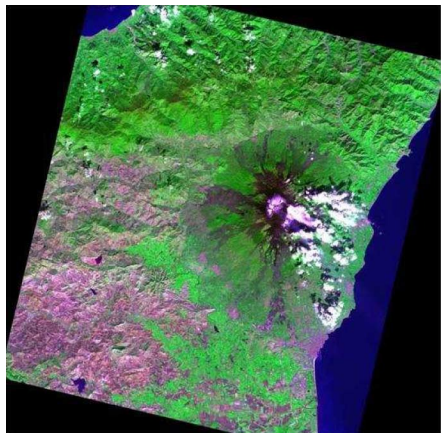

(a)

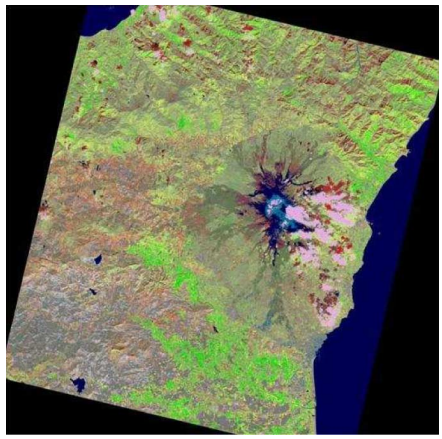

(b)

Fig. 5. (a) ALOS AVNIR-2 image of Sicily, Italy, in TOARF values, acquisition date: 2006-13-08, depicted in false colors (R: band 3, G: band 4, B: band 1). Spatial resolution: 10 m. (b) Output map, depicted in pseudo colors [same as in Fig. 2(b)], automatically generated by SRC from the image shown in Fig. 5(a).

[47], Richter writes that in the three optical sensors carried onboard the IRS-P6 platform, the bias "nominal value is zero... the calibration coefficient seem to be constant with time, i.e., independent of the scene, based on laboratory calibration".

Thus, according to this author's experience supported by Richter's observations, a list of currently ongoing European and non-European EO satellite optical imaging sensors series employing, in practice, absolute calibration zero-value offset parameters is provided below.

- SPOT-1/-2 High Resolution Visible (HRV).
- SPOT-4 High Resolution Visible & Infrared (HRVIR).
- SPOT-5 High Resolution Geometric (HRG), SPOT-4/-5 Vegetation Monitoring Instrument (VMI) 1 and 2, respectively.
- IRS-1C/-1-D Linear Imaging Self-Scanner (LISS-III).
- IRS-1C/-1-D low resolution Wide Field Sensor (WiFS).
- IRS-P6 medium resolution Linear Imaging Self-Scanner (LISS-III).
- IRS-P6 low resolution Advanced Wide Field Sensor (AwiFS).

Are SPOT and IRS zero-value offset parameters, apparently generated from laboratory calibration (according to the Richter conjecture), validated in terms of calibration quality and uncertainty in agreement with the QA4EO guidelines?

In a recent conversation which took place during the ESA-European Satellite Center (EUSC) Image Information Mining Coordination Group (IIMCG) Conference—Pursuing automation of geospatial intelligence for environment and security held at the ESA facility in Frascati (Italy) on March 4–6, 2008, one of the main research scientists involved with radiometric calibration of the SPOT satellite sensor series acknowledged technical difficulties in assessing the absolute calibration offset parameters of the SPOT-4/-5 imaging sensors ... [72]. This means that offset parameters provided by the SPOT sensor series should be considered unknown rather than null. In literature, Richter states that in the SPOT metadata files "the standard offset values are zero. Occasionally, however, for SPOT-4/-5 data a slightly negative offset has to be introduced for band 4 (1.6 μm, medium infra-red) in cases when the scene water reflectance is too high (it should be close to zero)" [47, p. 100]. In [40], it is stated that "the absolute calibration consists in estimating and monitoring the parameter $A(b)$ for the bth spectral band considered. Actually, for many applications, the most important thing is not the absolute calibration but the relative calibration between images

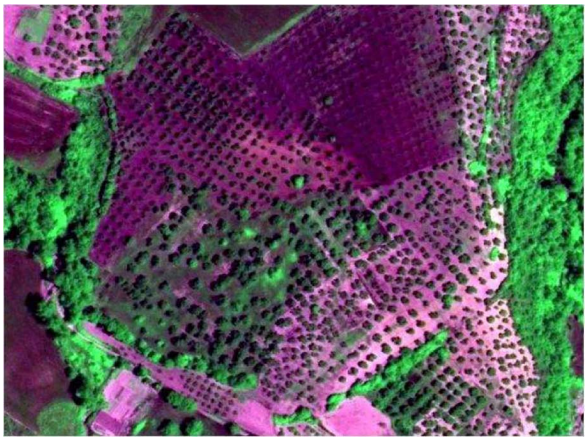

(a)

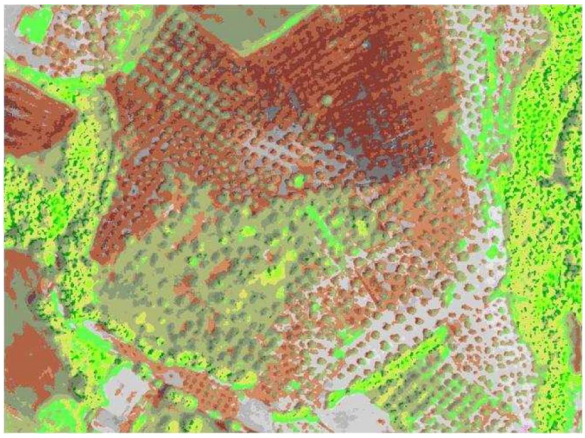

(b)

Fig. 6. (a) Zoomed image in TOARF values extracted from a QuickBird-2 image of Campania, Italy, acquisition date: 2004-13-06, 09:58 GMT, depicted in false colors (R: band 3, G: band 4, B: band 1), 2.44 m resolution, panchromatic-sharpened at 0.61 m resolution. (b) Output map, depicted in pseudo colors [same as in Fig. 2(b)], automatically generated by SRC from the image shown in Fig. 6(a).

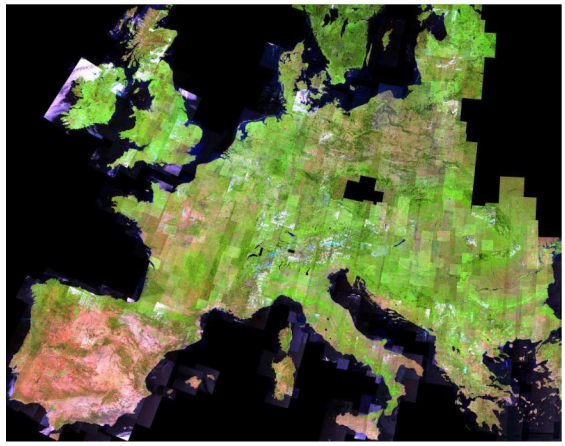

(a)

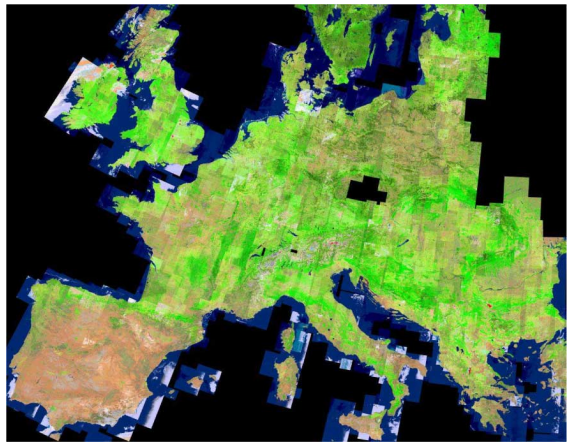

(b)

Fig. 7. (a) IMAGE2006 Coverage 1 mosaic, consisting of approximately two-thousand IRS-P6 LISS-III, SPOT-4 and SPOT-5 images, mostly acquired during 2006, radiometrically calibrated into TOARF values and geometrically orthorectified. Images are depicted in false colors: Red—Band 4 (Short Wave InfraRed, SWIR), Green-Band 3 (Near IR, NIR), Blue—Band 1 (Visible Green). Spatial resolution: 25 m. (b) Preliminary classification map of the IMAGE2006 Coverage 1 mosaic automatically generated by SRC from the image shown in Fig. 7(a) and depicted in pseudo colors [same as in Fig. 2(b)].

of the same instrument at different dates (multidate calibration), images acquired simultaneously in different spectral bands (interband calibration), images acquired by two different sensors (namely, SPOT-4 VEGETATION and HRVIR sensors intercalibration)". The author of this work, together with an anonymous referee, disagree with this quoted statement. In the words of this anonymous referee, "absolute calibration is the establishment of the "Gain" and "Offset," not simply a ratio" (generated from relative calibration)! In practice, the aforementioned statement taken from [40] would undermine the capability of implementing operational satellite-based measurement systems whose only requirement is the transformation of input DNs into a community-agreed radiometric unit of measure. In line with the Richter experience (refer to this text above) [47], this author has observed that in several SPOT-4 and SPOT-5 scenes radiometrically calibrated into TOARF values computed by (1) and (3) as a function of the absolute radiometric calibration parameters retrieved from the SPOT DIMAP metadata files, scene-derived land cover class-specific spectral signatures in TOARF values: (i) may fall well outside the range of change of the same land cover class-specific TOARF values detected across time and space by a plethora of spaceborne optical sensors listed in Table II and (ii) appear to be inconsistent with library or ground-measured surface reflectance spectra also considering that the latter are affected by no atmospheric effect [64], [65]. These two types of inconsistencies are illustrated in the following example representative of many similar cases personally experienced by this author.

Four open sea water-specific (equivalent to a dark-object) spectral signatures in TOARF values, shown in Table III, are extracted from the same region of interest located across a multisensor image dataset consisting of a Landsat-7 ETM+, one ASTER, one SPOT-5 HRG and one SPOT-2 HRV image of the Low Casamance mangrove ecosystem in Senegal acquired on, respectively, November 6th 2000, February 28th 2004, March 8th 2006 and March 1st 2006, see Figs. 8(a), 9(a), 10(a), and 11(a). In the target region of interest no sun glint phenomenon occurs, atmospheric scattering appears negligible in the visible and near infra-red (NIR) portions of the electromagnetic spectrum sensitive to the presence of haze and aerosols, whereas the amount of atmospheric scattering occurring at the medium

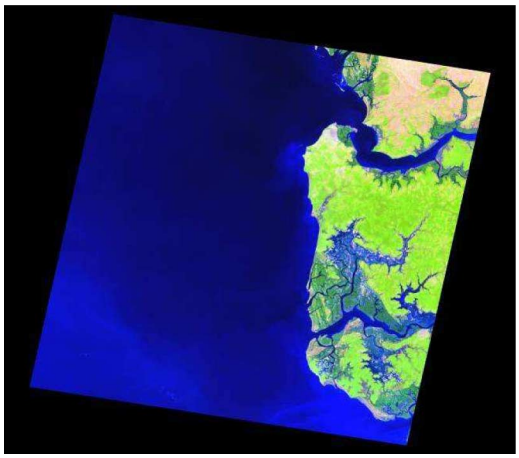

(a)

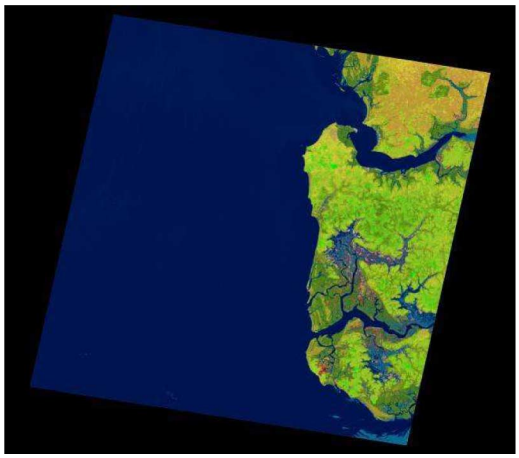

(b)

Fig. 8. (a) Landsat 7 ETM+ image of Senegal (path 205, row 051, acquisition date: 2000-11-06) in TOARF values, depicted in false colors (R: band ETM5, G: band ETM4, B: band ETM1), spatial resolution: 30 m. (b) Output map, depicted in pseudo colors [same as in Fig. 2(b)], automatically generated by SRC from the image shown in Fig. 8(a).

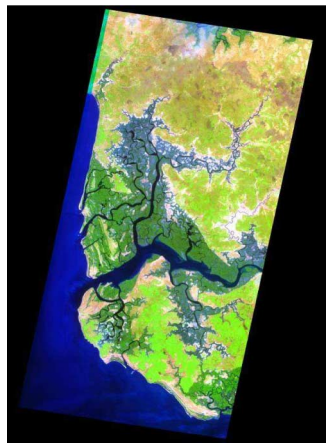

(a)

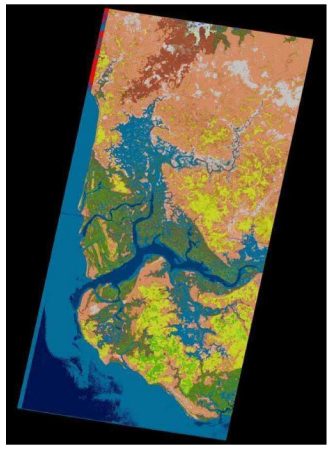

(b)

Fig. 9. (a) ASTER image mosaic of Senegal (acquisition date: 2004-02-28) in TOARF values, depicted in false colors (R: band 4, G: band 3, B: band 1), spatial resolution: 30 m. (b) Output map, depicted in pseudo colors [same as in Fig. 2(b)], generated by SRC from the image shown in Fig. 9(a).

infra-red (MIR) region of the spectrum is known to be "quite small except for very hazy atmospheres and can be considered negligible" [45, p. 476]. In Table III, the Landsat channels 1 to 7, identified as ETM1 to ETM7, are adopted as a reference in the comparison of multisensor channels featuring (approximately) the same sensitivity curve (e.g., a Landsat-like band 7 is synthesized by an OR combination of channels 5, 6, 7 and 8 by ASTER, refer to Table II). In other words, the author realizes that the spectral bandwidth of the individual bands affects the amount of at-sensor radiance, but differences in the spectral bandwidth are considered negligible here. In addition, intersensor TOARD and TOARF value comparisons should take calibration uncertainties into account, in agreement with guidelines for evaluating uncertainty of measurement found in the QA4EO documentation [66]. For example, the calibration uncertainties of the Landsat-7 ETM+ TOARD values are $\pm 5\%$ [67]. Unfortunately, in existing literature this author was unable to find any calibration uncertainty estimate for the ASTER and SPOT sensors involved with this comparison.

Table III shows that in the proposed qualitative example the sea water class (dark-object)-specific TOARF values provided by the SPOT-5 HRG sensor fall well outside the range of change of the corresponding TOARF values detected by the Landsat, ASTER and SPOT-2 optical sensors, which are more in line with the clear and turbid water reflectance values at the earth's surface found in existing literature (e.g., refer to [64, p. 273]). It is noteworthy that in Table III the relative increase in the band-specific SPOT-5 TOARF values with respect to the other sensors' values may be as high as 200% for band ETM2 up to 700% for band ETM5, which is far above the typical calibration uncertainty of spaceborne optical sensors (below 5% for the Landsat-7 ETM+ TOARD values, see this text above).

Overall, this author has observed that SPOT-4/-5 overestimation of TOARD/TOARF values may occur image-wide at varying geographic positions and solar elevation angles. Therefore, SPOT-4/-5 radiometric overestimation is not due to geometric effects or local surface conditions. In addition, this overcorrection is far superior to typical values of calibration uncertainty (see this text above). To summarize, the nature of SPOT-5 radiometric calibration inaccuracy appears to be accidental and scene-dependent, such as out-of-band leakage effects [68].

Experimental evidence of SPOT-5 radiometric inaccuracy can be automatically highlighted by the SRC approach (refer

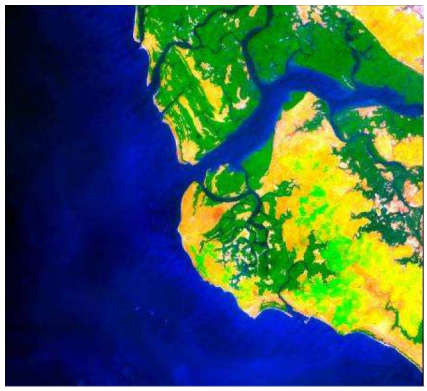

(a)

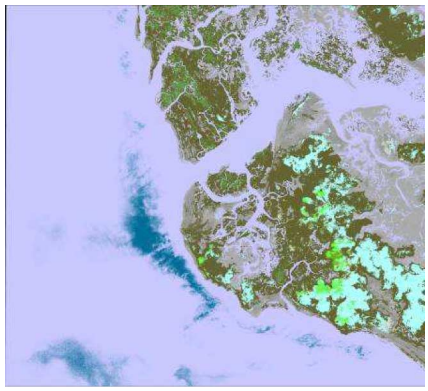

(b)

(c)

Fig. 10. (a) SPOT-5 image of Senegal (path 325, row 022, acquisition date: 2006-03-08) in TOARF values, depicted in false colors (R: band 4, G: band 3, B: band 1), spatial resolution: 10 m. (b) Output map, depicted in pseudo colors [same as in Fig. 2(b)], generated by SRC from the image shown in Fig. 10(a). Unknown pixels (outliers) are shown in red. Many water and ground pixels are mislabelled as spectral category thin cloud over water, depicted in light blue. (c) Output map, depicted in pseudo colors [same as in Fig. 2(b)], generated by SRC from the image shown in Fig. 10(a) after dark-object subtraction.

to Section III-B4 above). Shown in Fig. 10(b), the preliminary classification map automatically generated by SRC from the SPOT-5 image radiometrically calibrated into TOARF values [see Fig. 10(a)] looks meaningless (overall, many pixel-based spectral patterns [shapes] in TOARF values are either considered unknown or mislabeled by the SRC; for example, many water and ground pixels are assigned with the spectral label *thin cloud over water*). On the contrary, if a dark-object subtraction

(a)

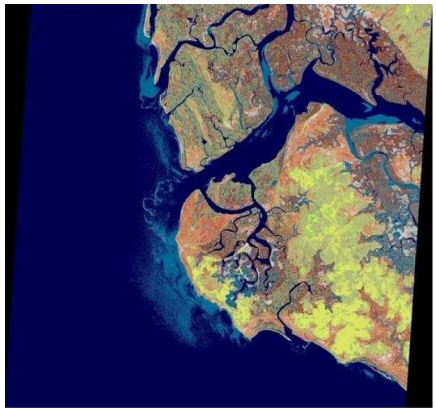

(b)

Fig. 11. (a) SPOT-2 HRV (High Resolution Visible) scene of Senegal in TOARF values, acquisition date: 2006-03-01, depicted in false colors (R: band 3, G: band 2, B: band 1). Spatial resolution: 20 m. (b) Output map, depicted in pseudo colors [same as in Fig. 2(b)], generated by SRC from the image shown in Fig. 11(a).

is employed in series with (1) and before (2), in line with [45], then the SRC map automatically generated from the SPOT-5 image, shown in Fig. 10(c), becomes consistent with the SRC maps generated from the radiometrically calibrated Landsat, ASTER and SPOT-2 images shown in Figs. 8(b), 9(b), and 11(b) respectively.

The conclusion that SPOT calibration quality and uncertainty are actually unknown may explain why, for example, the sole commercial operator of the SPOT satellites, SPOT Image, provides its SPOT product levels 1A (location root mean square [RMS] error <50 m), 1B (location RMS error <50 m), 2A (georeferenced to a standard map projection without using ground control points [GCPs], location RMS error <50 m), 2B (georeferenced with GCPs, location RMS error <30 m) and 3 (georeferenced with GCPs and orthorectified, location RMS error <15 m) with a geometric quality certification, but no radiometric quality index [41].

On the contrary, this conclusion is in contrast with SPOT commercial services where mosaics of co-registered orthorectified, but radiometrically uncalibrated SPOT images are sold to end users who may not be aware of the fact that these mosaics require a scene-by-scene understanding approach (because one scene represents, say, apples while the contiguous scene may represent oranges). This conclusion is also in contrast with

space agencies, such as the Flemish Institute for Technological Research NV (VITO), which continue to collect and analyze large-scale multitemporal SPOT observational data and to distribute derived information products without claiming that more progress on automating the classification of RS data requires continuous and traceable Cal/Val activity [71].

About the calibration quality of the IRS sensor series, Richter observed that in the three optical sensors carried onboard the IRS-P6 platform, the bias "nominal value is zero... the analysis of a couple of scenes showed that a nonzero bias is required to obtain reasonable surface reflectance spectra... A fine tuning of the calibration coefficients may be necessary to obtain better agreement between scene-derived surface reflectance spectra and library or ground measured spectra" [47, p. 104]. In line with this statement by Richter, this author has encountered several IRS image instances whose radiometric calibration quality appears troublesome. Nonetheless, based on experimental evidence collected over more than two-thousand SPOT and IRS images processed in the framework of the IMAGE2006 European mosaic project conducted by the EC-Joint Research Center (JRC) as part of the EU GMES Fast-Track Service Land Monitoring project [69], this author considers the IRS combination of zero-value offset parameters with nonzero gain parameters more effective overall than SPOT-4/-5's. As a consequence, in the IMAGE2006 mosaic IRS images have been preferred to SPOT-4/-5 imagery whenever the former were available and free of clouds, see Fig. 7.

In common practice, to recover from the aforementioned erroneous zero-value offset parameters, an additional relative calibration step is recommended in series with the SPOT-4/-5 (and maybe IRS) absolute radiometric calibration (1). For example, a user-driven standard dark-object subtraction, typically used to remove the additive atmospheric scattering (haze) effects [45], can be scheduled in series with (1) or (3), e.g., refer to [70]. In dark-object subtraction techniques, the DN to subtract from each band may be the band minimum, an average based upon a user-defined region of interest (typically, a water body of invariant spectral properties, a shadow area or a black object featuring 0% reflectance) or a specific value to be user-defined (e.g., selected from the DN frequency histogram of the whole RS image) [45], [65].

To summarize, a community-agreed RS data preprocessing protocol comprising a relative calibration step in series with the absolute radiometric calibration of SPOT-4/-5 (and maybe IRS) imagery should become mandatory to validate the unknown calibration quality of SPOT-4/-5 (and maybe IRS) data. Otherwise, this unknown radiometric quality should be dealt with by scene-by-scene data processing approaches unsuitable for applications such as:

i) quantitative estimates of either physical (e.g., LAI) or biochemical variables (e.g., Fraction of Absorbed Photosynthetically Active Radiation, FAPAR) such as those provided in the frame of the VEGETATION For Africa (VGT4AFRICA) project, led by the VITO, based on the SPOT-4/-5 VEGETATION sensor series [71];
ii) operational automatic generation of standardized, advanced and validated information products (e.g., classification maps) across time (e.g., image time series), space (e.g., image mosaics), and sensors in line with the GEOSS and GMES requirements;
iii) photointerpretation of image datasets across time and space in scientific applications such as land cover change detection at geographic scales ranging from local to global.

The obvious drawback of a SPOT-4/-5 (and maybe IRS) data processing chain which, to become eligible for use in an operational satellite-based measurement system, includes a manual or semi-automatic missing offset parameters retrieval sub-system is that its operational performance measurement becomes inferior to that of alternative spaceborne data sensors provided with complete and reliable absolute radiometric calibration offset and gain parameters.

To conclude, in agreement with the new QA4EO guidelines, the current vagueness about the SPOT and IRS calibration quality and uncertainty should be the subject of further inquiries by the RS community at the earliest opportunity and at the highest official level, such as the GMES bureau and the CEOS WGCV. On a personal basis, for the sake of truth and in the interest of the RS community involved with the development of operational satellite-based measurement systems, this author would personally welcome a comment by SPOT Image and the Indian Space Research Organisation (ISRO) about the aforementioned SPOT and IRS Cal/Val-related issues.

V. Comparison of the Radiometric Calibration Capabilities of European Versus Non-European Satellite Optical Sensors

The rationale of European Technology Platforms (ETPs) is to contribute to industrial competitiveness, boost research performance and provide a positive impact on EU's policies. Among possible fields suitable for long-term public-private partnerships, the GMES project was identified [73]. In the framework of ETPs, the EU Lisbon treaty explicitly aimed at fostering the competitiveness of EU industries. Is competitiveness of the European EO satellite industry undermined by inadequate Cal/Val strategies?

According to Section IV above, lack of one-of-two radiometric calibration parameters affects a currently ongoing European EO satellite optical sensor series, namely, SPOT-4/-5.

In addition, to date the German RapidEye constellation of five very high spatial resolution (VHR) satellites, successfully launched on September 6, 2008, does not appear to provide stakeholders with radiometrically calibrated images [74]. This latter case can be considered a relevant example of how an underestimation of the Cal/Val issue may reduce the commercial impact of RS optical imaging technology. In fact, on the one hand the unsurpassed one-day time resolution of the RapidEye satellite sensor constellation provides end users with multisensoral multitemporal sequences of VHR images. On the other hand, to compensate for differences in solar illumination and enhance multisensoral data consistency and comparability, the radiometric calibration of RapidEye image time series should be considered mandatory.

Finally, neither the ongoing Project for On-Board Autonomy (PROBA)-1 Compact High Resolution Imaging Spectrometer

(CHRIS) (20 m MS) nor the future PROBA-2 satellite, considered by ESA as a Third Party Mission to be launched in 2009, are provided with an onboard calibration system [75].

Based on the aforementioned considerations, it is possible to conclude that only a minority of currently ongoing EU satellite optical missions, namely, the EUMESAT METEOSAT 2nd Generation (MSG) Spinning Enhanced Visible and IR Imager (SEVIRI), the ENVISAT AATSR and the ENVISAT MERIS, appears to be provided with complete and more reliable onboard calibration systems. It is noteworthy that the future planned GMES Sentinel-2 (to be launched in October 2012) and Sentinel-3 optical missions will adopt the same onboard sun-based calibration system approach adopted by AATSR and MERIS.

With regard to the issue of EO data radiometric quality, a comparison of the aforementioned currently ongoing EU satellite optical missions with competing EO sensors developed by EU's global competitors may be rather difficult. For example, many, if not all, of the optical sensors mentioned in this text rely on vicarious calibration and it is not always clear how "official" and traceable Cal/Val activity is established to combine onboard and vicarious calibration results (e.g., in agreement with the QA4EO guidelines [37]). Although fuzzy, this comparison cannot be considered completely favourable to the EU optical sensors.

On the one hand, several non-EU platforms do not provide calibrated sensors, thus EU sensors cannot be considered behind in the global competition for EO data acquisition from space. To the best of this author's knowledge, examples of non-EU sensors affected by serious radiometric calibration problems are those of the CBERS-2B subsystems, namely, a CCD camera (bands 1–4) and an InfraRed Multi-Spectral Scanner (IRMSS, bands 5–7). This statement is not obvious.

1. It implies that for the time being CBERS-2B cannot be considered suitable for Landsat "gap-filling" which may become necessary before December 2012 when the next Landsat mission is due to be launched[6] [76].
2. It is somehow in contrast with the "perfect behavior" of the CBERS satellite series, which must not be intended in terms of sensor series, claimed in [77] where it is written that the "CBERS Program, in a first moment, considered two remote sensing satellites only, namely CBERS-1 and -2. The success of both launches, by the Chinese Long March 4B, and the perfect behavior of CBERS-1 and CBERS-2 had immediate effects. Indeed, both governments decided to expand the cooperation and include new satellites of the same class, CBERS-2B and CBERS-3 and 4, as a second stage of Sino Brazilian cooperation." It is noteworthy that in spite of their radiometric calibration problems, more than 700 000 CBERS images per year are distributed, free of charge, among RS scientists and practitioners by the Brazilian Instituto Nacional De Pesquisas Espaciais (INPE). Actually, these end users are willing to interpret costless noncalibrated RS imagery on a scene-by-scene basis for applications whose geographic extent may range, in practice, from local to regional scales exclusively [1], [78]. Follow-on missions to CBERS-2B, namely, CBERS-3 to -6, are expected to solve the radiometric calibration problems of CBERS-2B.

On the other hand, all the best-known United States (US) EO satellite optical missions, either ongoing or terminated, operated by either scientific institutions or private space companies, ranging from low to very high spatial resolution, such as the National Oceanic and Atmospheric Administration (NOAA) Advanced Very High Resolution Radiometer (AVHRR), the Moderate Resolution Imaging Spectroradiometer (MODIS) TERRA (EOS AM) and AQUA (EOS PM) sensors, Landsat-5 TM, Landsat-7 ETM+, IKONOS-2, QuickBird-2, OrbView-3, etc., feature either good or excellent radiometric calibration capabilities [13], [15], [16], e.g., see Figs. 3, 6, 8, and 9. For example, the ETM+ sensor has three onboard calibration devices for the reflective bands and has also been calibrated vicariously using Earth targets. The gain trends from the ETM+ sensor are regularly monitored on-orbit using the onboard calibrators and vicarious calibration. The calibration uncertainties of ETM+ at-sensor spectral radiances are $\pm 5\%$. Overall, ETM+ is the most stable of the Landsat sensors, changing by no more than 0.5% per year in its radiometric calibration [67]. This is one of the reasons why existing RS literature considers Landsat-5 TM and Landsat-7 ETM+ missions capable of providing data having tremendous scientific utility and the Landsat combination of spatial and spectral resolutions being fine enough to address most of the environmental and ecological problems and to map natural resources [80], which requires a follow-on mission to Landsat-7 [1, p. 451].

Furthermore, India's (in Section IV, refer to IRS versus SPOT) as well as Japan's EO satellite optical sensors (e.g., refer to ASTER and ALOS AVNIR-2 in Table II) appear to be at least not inferior to their European competing sensors in terms of claimed radiometric calibration capabilities that have been personally validated by this author (e.g., refer to Figs. 4, 5, 7, and 9).

To date, the author of this paper has been unable to assess the radiometric calibration properties of other non-European VHR satellite optical missions distributed through European companies such as the FORMOsa SATellite (FORMOSAT)-2 and the KOrean MultiPurpose SATellite (KOMPSAT)-2, both distributed by SPOT Image.

Overall, the aforementioned comments in combination with those in Section IV are in strong disagreement with potential options for Landsat "gap-filling" considered by USGS during the Landsat Science Team held at Fort Collins, CO, USA, on 6th–8th January 2009 [76]. If Landsat-5 fails in the coming months (after 25 years in operation a major system failure is considered very likely to occur within the year 2010), this failure would cause a time gap in the Landsat data coverage until the year 2013, since the follow-on Landsat mission should be launched in December 2012. In [76], eligible sensors

[6]Launched in April 1999, Landsat-7 ETM+ continues to acquire data globally. The Scan Line Corrector failure in April 2003 has affected ground coverage and the switch to Bumper Mode operations in April 2007 has degraded the internal geometric accuracy of the data, but the radiometry has been unaffected. Launched in March 1984, Landsat-5 TM+ continues to acquire global data. A technical failure of one of the transmitters in 1987 means that only data acquired within an acquisition circle of a ground station can be downlinked. The TM scanner was switched to Bumper Mode operations in April 2002, which has degraded the internal geometric accuracy of the data, but the radiometry has been unaffected [79]. A major system failure of the Landsat-5 TM mission is considered very likely to occur within the year 2010 [76].

for Landsat "gap-filling" are considered the CBERS-2B, the IRS-P6 AWiFS, the SPOT sensor series and the RapidEye constellation. This paper contradicts this statement by considering all these sensors unable to satisfy, to date, the demand for continuous traceable Cal/Val-related activities advanced by the new QA4EO initiative [19].

The timing of Landsat data availability is not fixed and the availability of future Landsat-like data is still a subject of debate, though the US intention is to make these data available free of charge in the same manner as Landsat. Thus, in agreement with the new QA4EO guidelines about Cal/Val-related activities, European space agencies and institutions should discuss their own Landsat "gap-filling" initiatives with the GMES bureau at the earliest opportunity [76].

VI. Other Sensor Specifications Causing an Increase in the Timeliness of Either Ongoing OT Future EU Satellite Optical Imaging Sensors

There are two more reasons that cause an additional reduction of the usability domain of SPOT imagery and, perhaps, of future EU satellite optical imaging sensors. In practice, these technical factors increase sensor timeliness (refer to the definition in Section II above).

A. Large Time Baseline Between PAN and MS Image Pair Acquisition

Ongoing SPOT-5 panchromatic (PAN, 2.5 m resolution) and MS (10 m resolution) imaging sensors do not acquire PAN and MS image pairs simultaneously, but about 3 sec apart which corresponds to a space baseline of some ($\approx$30) kilometers. For comparison, this time difference is equivalent to some fractions of a second in both IKONOS-2 and QuickBird-2 satellite sensors whose PAN and MS image spatial resolutions are, by the way, finer (i.e., better) than SPOT-5's, see Table II. This problem causes any SPOT-5 MS image PAN-sharpening attempt to be affected by huge visual "terrain effects" if no preliminary pixel-by-pixel co-registration of the SPOT-5 PAN and MS image pair is performed. Unfortunately, a SPOT-5 PAN and MS image pair co-registration process featuring a standard co-registration error below 1/2–1/5 of a pixel [81], [82], may become extremely difficult in real-world RS data applications, e.g., when a typical SPOT-5 image size is 24000×24000 pixels and when the image depicts terrain areas where it is difficult to detect conjugate point pairs (e.g., mountainous areas covered by snow) [15].

To summarize, by requiring relative calibration in series with the absolute radiometric calibration (refer to Section IV above) in addition to MS and PAN image pair co-registration before MS image PAN-sharpening takes place, SPOT-5 is affected by a timeliness far superior to that of its rival VHR sensors, namely, IKONOS-2, QuickBird-2, etc.

It is noteworthy that in the Astroterra system characteristics of the follow-on missions to SPOT-5, namely, Astrium's SPOT-6/-7 to be launched in 2012 and 2017 respectively, simultaneous PAN and MS image acquisition is planned [83].

B. Change in Spectral Resolution Causing an Increase in Inter—Band Data Correlation and Sensitivity to the Presence of Haze and Aerosols

In the near future the fourth generation of EO satellite sensors should move towards the FIEOS paradigm (refer to Section III-A above) where onboard automatic data processing capabilities require RS data to be well behaved and well understood (also refer to Sections I and II above) [49]. To satisfy the operational requirements of FIEOS, future planned RS imaging sensors should carefully balance an increase in spatial resolution with changes in spectral resolution which may have a negative impact upon the implementation of operational satellite-based measurement systems. A reasonable criterion to assess a novel combination of spatial and spectral sensor resolutions should start from existing literature, where the Landsat-5 TM and Landsat-7 ETM+ combination of spatial and spectral resolutions is considered a reference standard, fine enough to address most of the environmental and ecological problems and to map natural resources [80].

In spite of these considerations, the design characteristics of future European EO satellite optical imaging sensors appear to move away from both the Landsat sensor characteristics and, perhaps, the FIEOS scenario as discussed below.

The satellite constellation Pleiades-1/-2, to be developed by the French Space Agency (Centre National d'Etudes Spaciales, CNES) by the year 2009 and 2012 respectively, featuring PAN spatial resolution equal to 0.60 m and MS spatial resolution equal to 2.8 m at nadir, and the follow-on missions to SPOT-5, namely, Astrium's SPOT-6/-7 to be launched in 2012 and 2017 respectively, featuring PAN spatial resolution equal to 2 m and MS spatial resolution equal to 8 m at nadir [83], lose the MIR channel of the SPOT sensor series in favour of a visible blue (B) band [84]. This change in spectral resolution implies that:

1. Pleiades-1/-2 and SPOT-6/-7 will become alternative to a plethora of VHR sensors such as GeoEye-1, IKONOS-2, QuickBird-2, OrbView-3, FORMOSAT-2, KOMPSAT-2, etc., featuring the same spectral resolution (see Table II). Unfortunately, the future Pleiades-1/-2 spatial resolution is expected to be coarser than that of some of its non-EU rivals already in orbit (e.g., GeoEye-1).
2. Irrespective of spatial resolution, the (spectral) information content (amount of information) of a 4-band Pleiades image is expected to be inferior to that of a 4-band SPOT-4/-5 image of the same depicted surface because the interband correlation of the former sensor is superior. This is tantamount to saying that the spectral separability of potential targets decreases in MS images acquired by the Pleiades imaging sensor in comparison with ongoing SPOT-4/-5's. Moreover, the MIR channel to be lost in the Pleiades optical sensor has been described as the best band overall [70]. Its wavelengths are sensitive to water absorption and, as such, it is useful for vegetation moisture content, soil moisture and soil versus vegetation differentiation, as well as snow versus cloud discrimination. In combination with a Near-IR (NIR) channel it was largely employed to compute so-called bare soil spectral indexes [15], [60], [85].

3. It is well known that light scattering due to atmospheric conditions and aerosols is inversely proportional to the energy wavelength λ, i.e., shorter wavelengths of the spectrum are scattered more than the longer wavelengths (refer to Section III-A above). For example, in the MIR wavelengths the amount of atmospheric scattering is known to be "quite small except for "very hazy" atmospheres and can be considered negligible" ([45], p. 476). For example, the well-known Landsat-7 ETM+ automatic cloud cover assessment (ACCA) algorithm considers band B of limited utility because of its sensitivity to scattering across atmospheric conditions. Therefore, it ignores this band in cloud detection [38]. Analogous to ACCA, the fully automated SRC system of systems (refer to Section III-B4 above) is designed to be scarcely affected by atmospheric scattering by taking visible bands into scant consideration [15], [60]. In practice, weights of visible channels are low in the SRC decision rules based on a convergence-of-evidence mechanism. The only case in which SRC considers band B very useful (i.e., provided with great weight) is the generation of haze and aerosols binary output masks [15].
4. In line with theoretical considerations 2 and 3 expressed above, SRC experimental results gathered in [15], [16] show that replacing a MIR band with a B band causes (when spatial resolution is maintained the same): (i) a significant reduction in the cardinality of the set of target spectral categories, estimated at about 30%, and (ii) a consistent reduction in the reliability of target spectral categories, starting from a mislabeling probability above 10% in the dichotomous one-class vegetation/nonvegetation image partition problem.

The obvious conclusion is that, in comparison with the currently ongoing SPOT sensor series, the future planned Pleiades and SPOT missions gain in spatial resolution, but are moving farther away from the development of the onboard automated image processing capabilities required by the FIEOS scenario and from the spectral resolution of the Landsat missions considered the most successful EO satellite optical sensor series.

VII. Lack of Operational RS Image Understanding Systems due to the Omission of a Radiometric Calibration Preprocessing Stage

In this section, Cal/Val activity is investigated in EO data research and development projects carried on in recent years by the ESA and the EC-JRC adopted as two case studies. Since these two EU institutions are deeply involved with the GMES program and have been members of the CEOS for more than twenty years, it would be reasonable to expect these two institutions to consider radiometric calibration an essential preprocessing component of operational RS-IUSs in agreement with the new QA4EO initiative.

A. First Case Study: ESA

ESA is the coordinator of the space component of GMES and is ensuring the flow of EO data into the GMES services along with access to these data [23]. However, to face the challenge of implementing operational satellite-based measurement systems, ESA should not limit its efforts to the harmonization of the GMES data flow and data access. Rather, in agreement with this text above, ESA should also ensure that all the acquired data can be assembled into image time series and/or image mosaics of consistent radiometric and geometric quality at different spatial scales. In other words, to guarantee interimage comparability across time, space and sensors, ESA should require the operators of contributing satellite missions to apply operational, standardized, consensus-based image preprocessing operations according to the following sorted sequence.

1. Radiometric calibration. It is noteworthy that RS image radiometric calibration should be performed before orthorectification and co-registration and not the other way around. The reason is twofold. First, transformation of raw DNs into a finite radiometric scale such as TOARF values in range [0, 1] allows checking for radiometric consistency of pixel values after image orthorectification and co-registration take place. Second, radiometric metafiles report the raw image size (in lines and columns) which does not hold after that orthorectification and co-registration occur. In other words, on the one hand, to perform radiometric calibration in series with orthorectification and co-registration, two ancillary metafiles (or file headers) should be read instead of a single one. On the other hand, to perform radiometric calibration before orthorectification makes no difference to the latter.
2. Orthorectification (which requires an ancillary digital terrain model).
3. Co-registration.
4. Atmospheric correction (which requires ancillary data), if any [47], [61], refer to Section III-A above.
5. Topographic correction (which requires an ancillary digital terrain model [62]), if any.

To date, lack of ongoing RS image preprocessing protocols shared between ESA and its EU institutional partners, such as the DLR and the EC-JRC, together with insufficient data management and data sharing policies, has had dramatic consequences. For example, in the framework of the GMES IMAGE2006 component and development of the European mosaic project between ESA, DLR and the EC-JRC [69], SPOT-4 HRVIR, SPOT-5 HRG and IRS-P6 LISS-III MS images acquired across the European geographic extent were orthorectified by DLR without applying any preliminary radiometric calibration step (which is inconsistent with the RS image preprocessing protocol proposed above in this text). Next, these orthorectified images were delivered by DLR to the ESA and the EC-JRC. However, the original IMAGE2006 raw data calibration metafiles generated by the SPOT and IRS data providers were made available to the DLR and EC-JRC exclusively. In other words, the ESA IMAGE2006 online archive consists of orthorectified images provided with no radiometric calibration metadata. As a consequence, in the framework of the ESA Category 1 data free access policy [87], scientific users are unable to transform the orthorectified images belonging to the IMAGE2006 dataset at continental scale into a common radiometric scale. This occurs despite the ESA, DLR and EC-JRC are members of the CEOS which officially supports the QA4EO initiative and in spite of the well-known principle that data management, including data sharing and redundancy

(duplication), is often more critical than data collection in guaranteeing the integrity (i.e., accuracy and completeness) of a database [88].

It is hoped that following implementation of the new QA4EO guidelines, where ESA has a leading role, access to an ESA IMAGE2006 online archive comprising complete RS data with radiometric calibration metadata files will be made available to stakeholders in the short term.

B. Second Case Study: EC-JRC

In recent years the EC-JRC has been conducting a plethora of RS image research and development activities aimed at supporting EC policies that range from environment and sustainability issues, such as global land cover and land cover change mapping of RS image mosaics [25], [28], to protection and security issues, such as built-up damage assessment and refugee camp monitoring in VHR imagery [89]. Quite surprisingly, most of these investigations have inferred quantitative information from input RS images acquired across time and/or space and/or sensors that have never been preprocessed into a common unit of measure belonging to an international system of radiometric units. Some examples of these scientific studies are summarized below.

a) Applications for the Environment and Its Sustainability: In [25] the IMAGE2000 and CORINE Land Cover (CLC) updating for the year 2000 (CLC2000) project delivered twenty-nine (!) national mosaics and one European mosaic consisting of 25 m-resolution orthorectified Landsat-7 ETM+ images featuring a Root Mean Square Error (RMSE) of $\approx$25 m. No radiometric calibration requirement was adopted in the IMAGE2000 project specification. This implies that firstly the IMAGE2000 mosaics at national and continental scales were generated on a scene-by-scene basis either manually or, at best, semi-automatically at a high cost in terms of manpower. Secondly, the radiometric quality of the IMAGE2002 is unsuitable for use in operational satellite-based measurement systems. This application example is particularly significant because, despite the fact that the radiometric calibration of Landsat imagery is particularly straightforward and effective, hundreds of RS scientists in twenty-nine (!) EU nations completely ignored any radiometric calibration preprocessing requirement in the context of RS image mosaicking at continental scale. This omission may be justified by considering that back in the 1990s, when the IMAGE2000 project requirements were set, the main issues were probably data distribution and result dissemination rather than raw image transformation into a radiometric unit of measure.

In [26], the Global Land-Cover (GLC)-2000 is a global mosaic for the year 2000 consisting of SPOT-VGT images at 1-km resolution. About data radiometry, it states that "absolute sensor calibration is in the order of 5%, while temporal variation is less than 2% for visible and near-infrared bands. This is achieved by using the onboard calibration lamp together with measurements in specific conditions over reference targets. Equalization between detectors in each array is monitored every 2 weeks and equalization function parameters are uploaded to the instrument processor for on-board correction. While this process is fully satisfactory for visible and near-infrared channels, it is not sufficient for the short-wave infrared camera whose detectors are randomly damaged by proton impacts. As a result, short-wave infrared images often display stripes corresponding to detectors damaged shortly after the updating of the on-board equalization functions." In practice, the GLC-2000 project appears to completely ignore radiometric calibration issues addressed above in this paper. As a consequence, no operational land cover mapping algorithm can be applied to images acquired across time and space that do not belong to a common radiometric scale. In fact, the GLC2000 project adopts a so-called "regionally tuned" approach where each regional product is generated "independently with the lead scientists taking responsibility for the choice and implementation of image postprocessing and classification methods". This is tantamount to saying that the GLC2000 image mosaic has to be classified on a scene-by-scene basis (one scene representing apples, another oranges, etc.).

In [27], the IMAGE2006 mosaic at European scale consists of SPOT-4/-5 and IRS-P6 LISS-III imagery, see Fig. 7 and refer to Section IV and Section VII-A above. Wherever available and free of clouds, the latter is preferred to the former, see Section IV above. IMAGE2006 employs a RS image absolute radiometric calibration preprocessing stage, but it completely ignores the lack of radiometric calibration offset parameters discussed in Section IV above. Additional critical issues related to the IMAGE2006 data management and data sharing policy among the ESA, EC-JRC and DLR are discussed in Section VII-A above. It is noteworthy that the complete omission of a radiometric calibration preprocessing stage affecting the IMAGE2000 mosaics was, at least in part, corrected in the IMAGE2006 project where, however, only one-of-two per band radiometric parameters is available and employed for calibration without validation. This reveals that in the last 10 years or so the issue of calibration has gained some positions, perhaps not as many as necessary, on the agenda of EU space agencies and research institutions.

In [28], where technical capabilities for monitoring deforestation in a pan-tropical scale are reviewed, keywords "radiometric calibration/normalization/processing" are used only once to state that "more recently new global land cover datasets at finer resolution (250–500 m) were generated from TERRA-MODIS... Initial examples at this scale include the MODIS vegetation continuous fields (VCF) products depicting sub-pixel vegetation cover traits at a spatial resolution of 500 m. The systematic geometric and radiometric processing of MODIS data has enabled the implementation of operational land cover characterization algorithms of global VCF tree cover. These are now available to researchers and are being incorporated into various forest cover and change analyses." In this quotation, the statement "the systematic geometric and radiometric processing of MODIS data has enabled the implementation of operational land cover characterization algorithms" is of fundamental importance. This operational issue is not stressed any further in [28]. Rather, it is perfectly in line with this paper where it states that radiometric calibration is a necessary, although not sufficient, condition for development of operational automatic RS-IUSs (see Sections I and II above).

It is even more amazing that in a paper dealing with the harmonization of global land cover maps, where one of the co-authors was a former member of the CEOS WGCV, the keyword "radiometric calibration" never appears [30].

Finally, it is noteworthy that in another global land cover project, namely the GlobCover joint initiative of the ESA, the EC-JRC and several other public institutions, an operational service capable of delivering global composite and land cover maps using as input observations from the 300 m MERIS sensor onboard the ENVISAT satellite mission was developed [29]. The GlobCover service was shown over a period of 19 months [December 2004–June 2006], for which a set of MERIS Full Resolution (FR) image composites (bi-monthly and annual), radiometrically calibrated into surface reflectance values, and a Global Land Cover map is being produced. The GlobCover composites are derived from a set of MERIS FR image processing modules such as cloud detection, atmospheric correction, geolocalization and re-mapping. The GlobCover Land Cover map is compatible with the United Nations (UN) Land Cover Classification System (LCCS). Unfortunately, almost nothing is known about the MERIS image understanding algorithm and its degree of automation [29]. Since no information is provided to application developers for the MERIS image understanding system to be reproduced, no assessment and comparison of this black-box image mapping approach with alternative systems is possible to date. This is tantamount to saying that this MERIS image classifier, provided with no documented community-agreed quantitative OPI (refer to Section II above), disagrees with the QA4EO guidelines.

b) Applications for the Protection and Security of the Citizen: Risk management involves both prevention, such as mapping of hazardous areas, and *a posteriori* evaluation of damaged areas. To provide fast-response (within few hours) actions imposed by Civil Protection entities, risk management implies real-time monitoring [2]. An operational spaceborne RS system for risk management must satisfy the following system requirements [15].

- A satellite constellation specific for the purpose of risk management. In particular:
  - — The revisit time (time period between two acquisitions on a given site) must be suitable for real-time monitoring, ranging from few hours to one day.
  - — On a case-to-case basis, spatial resolution and the spatial coverage must be appropriate for the required application. In general, the finest spatial resolution (<5 m) is required for monitoring man-made objects whereas characteristic spatial scales of urban areas are between 10 and 20 m [48].
- A satellite acquisition selection and programming procedure must introduce a time delay compatible with satellite revisit time.
- Cartographic products (maps of hazardous and damaged areas) of validated quality generated from the satellite data must be made available with the shortest time delay from data acquisition on a case-to-case basis. To reduce this time delay, the implementation of operational satellite-based measurement systems robust across time, space and sensors, which rely upon the availability of RS satellite data of demonstrably traceable and validated geometric and radiometric quality, becomes mandatory (see sections above in this text).

In the framework of risk management, algorithms found in existing literature appear far more suitable for toy problems and academic speculations than real-world RS data applications. For example, in [89], a built-up damage detection methodology uses as input two multiscale and multisensor VHR QuickBird-2 MS and PAN image pairs of the same area acquired before and after a catastrophic event (tsunami). Run upon this single testing dataset, the proposed methodology is claimed to reach an overall accuracy of 93.97%, with best performance in the discrimination between nonflooded and flooded built-up structures and in the recognition of collapsed built-up structures with debris in place. Indeed, a classification algorithm using as input a specific combination of multiscale multisensor multitemporal images not belonging to a common radiometric scale offers no guarantee of robustness to changes in the input dataset. By avoiding any investigation of the proposed system's robustness to changes in the input dataset, paper [89] fails to satisfy at least one of the following algorithm benchmarking criteria proposed in [90] and [91].

- At least two real and standard/appropriate data sets must be adopted to demonstrate the potential utility of an algorithm,
- The proposed algorithm must be compared against at least one existing technique.
- At least one fifth of the total paper length should be devoted to evaluation.

In [92], a procedure for the calculation of a 2nd-order statistic rotation-invariant contrast index extracted from a single-scale gray-level co-occurrence matrix (GLCM) is presented as a "built-up presence index" estimator. The proposed 2nd-order contrast statistic estimator is employed in a multitemporal analysis of a mosaic of SPOT-5 PAN images at 2.5 m resolution. This approach for detecting changes in textured images has several theoretical limitations which may reduce its robustness to changes in the input dataset.

i) This work completely ignores the radiometric calibration preprocessing requirement mandatory in multitemporal image analysis.
ii) The third-order version of the Julesz conjecture states that if two textured images of finite size have identical third-order statistics (which implies identical second- and first-order statistics), then they must be physically identical, i.e., they are visually undistinguishable by definition. In other words, third- rather than second-order statistics should be investigated in texture analysis [93]–[95].
iii) Texture detection, such as (textured) image decomposition, is a multiscale rather than single-scale image processing task [96], [97].
iv) The implemented 2nd-order contrast statistic estimator is a general-purpose (nonselective, non-"intelligent") texture feature extractor by no means sensitive to built-up areas exclusively. Therefore, its name, "built-up presence index", appears quite misleading.

To conclude, the aforementioned drawbacks identify RS image understanding approaches unsuitable for operational applications in risk management.

TABLE III

ON THE X-AXIS: EQUIDISTANT BAND INDEXES MONOTONICALLY INCREASING WITH SPECTRAL WAVELENGTH, FROM VISIBLE BLUE TO MEDIUM INFRA-RED (ALSO REFER TO TABLE II). ON THE Y-AXIS: TOARF VALUES IN RANGE [0, 1] × 100 OF OPEN SEA WATER SPECTRAL SIGNATURES EXTRACTED FROM THE SAME SEA WATER REGION OF INTEREST LOCATED ACROSS THE FOUR RS IMAGES SHOWN IN FIGS. 8(A), 9(A), 10(A), AND 11(A). ABOUT THE ADOPTED NOTATION, ETM1 IDENTIFIES A LANDSAT-7 ENHANCED THEMATIC MAPPER (ETM) BAND 1-LIKE IMAGE, AND SO ON, UP TO BAND ETM7, RANGING FROM VISIBLE BLUE TO MEDIUM INFRA-RED, WHEREAS BAND ETM6, DEALING WITH THE THERMAL INFRA-RED, IS OMITTED. FOR EXAMPLE, A SPOT-2/-5 BAND 1 IS APPROXIMATELY EQUIVALENT IN TERMS OF SPECTRAL SENSITIVITY CURVE TO ETM2, AN ASTER BAND 1 IS EQUIVALENT TO ETM2, ETC.

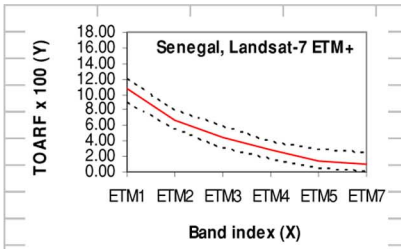

Senegal, Landsat-7 ETM+, 2000-11-06			
X	*Min Y*	*Max Y*	*Mean Y*
ETM1	9.00	12.00	10.68
ETM2	5.50	7.80	6.70
ETM3	3.10	5.88	4.44
ETM4	1.56	3.92	2.90
ETM5	0.40	2.74	1.32
ETM7	0.00	2.35	0.97

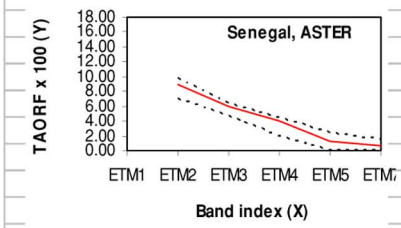

Senegal, ASTER, 2004-02-08			
X	*Min Y*	*Max Y*	*Mean Y*
ETM1			
ETM2	7.00	9.80	9.00
ETM3	4.70	6.40	5.88
ETM4	2.00	4.50	4.00
ETM5	0.00	2.30	1.24
ETM7	0.00	1.50	0.72

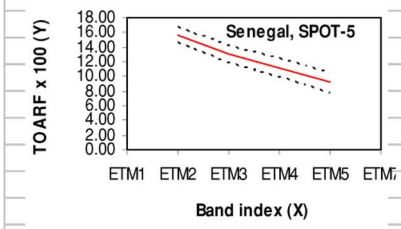

Senegal, SPOT-5, 2006-03-08			
X	*Min Y*	*Max Y*	*Mean Y*
ETM1			
ETM2	14.50	16.80	15.67
ETM3	11.70	14.10	13.05
ETM4	9.80	12.50	11.25
ETM5	7.80	10.50	9.17
ETM7			

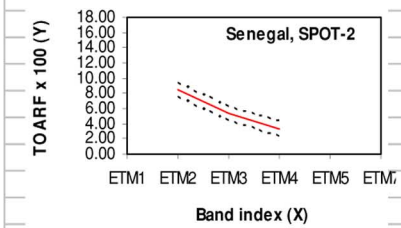

Senegal, SPOT-2, 2006-03-01			
X	*Min Y*	*Max Y*	*Mean Y*
ETM1			
ETM2	7.45	9.41	8.51
ETM3	4.31	6.27	5.40
ETM4	2.35	4.31	3.35
ETM5			
ETM7			

C. Final Remarks About the Two Case Studies

All the aforementioned RS image applications, aside from those dealing with radiometrically calibrated data, namely, the MODIS VCF project and the GlobCover initiative, cannot rely upon operational automatic land cover mapping algorithms, but either "regionally tuned" or scene-by-scene classification procedures.

In practice, underestimation of the radiometric calibration preprocessing stage forces the development of scene-by-scene classification and postprocessing procedures whose costs in terms of manpower (which includes the collection of ground truth data, if any), RS data processing expertise of human operators and timeliness increase monotonically with the size of the image mosaic. For these reasons scene-by-scene interpretation approaches have been featuring a negligible impact upon both scientific and commercial RS data applications. As reported in Section II above, to date only 10% of the RS data stored in the ESA EO archives has ever been downloaded by stakeholders [24], while the percentage of the literally hundreds of so-called novel digital image processing algorithms presented each year in scientific literature that are actually implemented in commercial RS image processing software toolboxes still remains far below reasonable expectations [10].

VIII. CONCLUSION

Although often ignored in RS common practice, continuous traceable Cal/Val-related activities, well defined and controlled

through community-agreed reference standards in accordance with the new GEO-CEOS WGCV QA4EO initiative, are considered crucial in achieving harmonization and interoperability of EO data and derived information products generated from a variety of sources at all scales—global, regional and local—as envisaged under the visionary goals of the well-known GEO-GEOSS and GMES programs. The original contribution of this work to existing knowledge on the Cal/Val subject is to consider, based on existing literature, continuous traceable Cal/Val activities, from sensor build to end-of-life, a necessary, although not sufficient, condition for development of operational automatic RS-IUSs requiring as input RS images that are well behaved and well understood, namely, sensor delivered data that are: (i) calibrated into a physical unit-of-measure related to a community-agreed radiometric scale and (ii) validated in terms of radiometric and geometric quality.

As a consequence, this paper delivers a timely reminder to the space agencies and commercial satellite industries of their responsibility to provide the scientific and commercial communities with radiometrically calibrated RS data of validated geometric and radiometric quality suitable for use in operational satellite-based measurement systems.

It is noteworthy that the degree of match of the radiometric calibration characteristics of ongoing EU spaceborne missions with Cal/Val guidelines promoted by the new QA4EO initiative is either low or very low. For example, experimental evidence collected by this author reveals that the calibration quality of the absolute radiometric calibration metadata of SPOT-4/-5 (and maybe IRS) imaging sensors appears to be questionable. Despite being neglected by the RS community, this subject deserves further scientific investigation at institutional level. Other ongoing EU spaceborne missions, such as RapidEye and PROBA, appear to deliver EO data that are not radiometrically calibrated and, therefore, validated in terms of calibration quality and uncertainty as required by the QA4EO initiative. As such, they are not eligible for use in operational automatic RS-IUSs.

In comparison with ongoing SPOT-4/-5 sensor characteristics, future planned EU Pleiades-1/-2 and the follow-on Astrium's SPOT-6/-7 missions will feature a finer spatial resolution capability, counterbalanced by a change in spectral resolution that is expected to increase their interband data correlation and sensitivity to the presence of haze and aerosols. This work estimates that in comparison to SPOT-4/-5, Pleiades-1/-2 and Astrium's SPOT-6/-7 may be affected by a spectral information loss responsible for: (I) a significant reduction in the cardinality of the set of target spectral categories, estimated at about 30%, and (II) a consistent reduction in the reliability of target spectral categories, starting from a mislabeling probability above 10% in the dichotomous one-class vegetation/nonvegetation image partition problem.

Unfortunately, little is known about the Cal/Val requirements of future planned EU spaceborne optical imaging sensors. For example, it is known that the Sentinel-2/-3 missions developed in the frame of the GMES project will adopt the same sun-based onboard calibration system technology employed by AATSR and MERIS. What about the radiometric calibration characteristics of Pleiades-1/-2 and the follow-on Astrium's SPOT-6/-7 missions? If these future EU satellite missions will not be able to satisfy Cal/Val reference standards in agreement with the QA4EO initiative, they may be considered unfit to support an operational, automatic, consensus-based and standardized RS data processing chain robust to changes in input data acquired across time, space and sensors. In other words, the radiometric quality of these satellite missions would be inadequate to deal with the major scientific challenges to the RS community within the next 10 years, such as the following.

- Achieving the visionary goal of developing operational GEOSS and GMES system instantiations.
- Providing Landsat "gap-filling", if required.
- Addressing the FIEOS development scenario where operational near real-time satellite-based measurement systems should be implemented.
- Reversing statistics according to which, to date, only 10% of the data stored in the ESA EO databases has ever been downloaded by stakeholders.
- Fulfilling many of the resolutions arising from international ecological, economic and social summits, such as the Johannesburg World Summit on Sustainable Development (WSSD) held in August 2002, calling for better utilization of cartographic solutions as well as other geo-information solutions, such as satellite mapping services, to monitor key bio-geo-physical processes and their changes at geographic scales ranging from local to global.
- Fulfilling many of the resolutions arising from ETPs and the EU Lisbon treaty aimed at fostering the competitiveness of EU industries.

In practice, if not provided with complete and reliable radiometric calibration metadata in agreement with the international QA4EO initiative, MS images generated from future EU satellite optical missions will be almost exclusively suitable for either scene-by-scene quantitative interpretation or nonscientific qualitative (visualization) applications in commercial internet map servers or geo-browsers such as Google Earth, NASA's World Wind and Microsoft's Virtual Earth whose popularity has become impressive in recent years [98]. It is noteworthy that the aim of commercial web-based map servers and geo-browsers is not RS image visual interpretation, but to use geography as a way of searching and viewing spatial information, i.e., to search for information provided with a geographic footprint [99]. As a consequence, these commercial web-based services require as input 3-band Red-Green-Blue (RGB) images in either natural or false colors featuring little to no scientific utility. This convergence of interests between the EO space industry, internet service providers and value adding companies is confirmed by a recent announcement that SPOT Image was named a Google Earth Enterprise Partner. In this new partnership with Google, SPOT Image will deliver "ready-to-use" image datasets (perhaps consisting of RGB images in either natural or false colors provided with no scientific utility?) for Google Earth and Google Earth Enterprise users to integrate the information content of SPOT satellite imagery into web-based Google Maps (2-D) and Google Globe (3-D) services [100].

Unfortunately, should their application domain be limited to commercial nonscientific qualitative (rather than quantitative) web-based services, future EU satellite optical missions, such as

Pleiades-1/-2 and Astrium's SPOT-6/-7, appear to be less competitive than their alternative non-EU satellite optical sensors already in orbit (e.g., GeoView-1) in terms of spatial resolution.

To avoid these potential drawbacks, a relevant section of the RS community committed to the development of operational automatic RS-IUSs should urgently require future planned EU satellite optical missions to be subject to a continuous, traceable, well-defined and controlled through community-agreed reference standards Cal/Val activity, in agreement with the QA4EO initiative, to become eligible for use in an operational GEOSS and GMES framework and for Landsat data "gap-filling", if required.

Finally, this work shows that several recent or ongoing European projects focusing on global land cover and land cover change, risk management and fast reaction to catastrophic events where EO satellite optical images are examined across time, space and sensors, neglect the transformation of raw DNs into a common radiometric unit of measure. In practice, EU space agencies and scientific institutions that, in recent years, have underestimated the importance of Cal/Val-related activities for EO data quality assurance in spite of their twenty-year membership in the CEOS show their reluctance (inadequacy?) to move from scientific to operational EO data applications. It is hoped that following implementation of the new QA4EO guidelines the development of operational automatic RS-IUSs, capable of accomplishing many of the resolutions arising from the GEOSS and GMES programs, will become a reality in a timely manner.

ACKNOWLEDGMENT

The author would like to thank the Editor-in-Chief, the Associate Editor, and anonymous reviewers for their support and helpful comments. The author praises their competence and willingness to help.

REFERENCES

[1] *Land Change Science* G. Gutman, Ed. *et al.*, Dordrecht, The Netherlands: Kulwer, 2004.

[2] F. Sart, J. Inglada, R. Landry, and T. Pultz, "Risk management using remote sensing data: Moving from scientific to operational applications," in *Proc. SBSR Workshop*, Brasil, Apr. 23–27, 2001 [Online]. Available: http://www.treemail.nl/download/sarti01.pdf

[3] [Online]. Available: http://www.fabricadebani.ro/userfiles/GEO_press_release.doc.

[4] O. Sjahputera, C. H. Davis, B. Claywell, N. J. Hudson, J. M. Keller, M. G. Vincent, Y. Li, M. Klaric, and C. R. Shyu, "GeoCDX: An automated change detection and exploitation system for high resolution satellite imagery," presented at the Int. Geoscience and Remote Sensing Symp. (IGARSS) Boston, MA, 2008.

[5] *GEO Announces Free and Unrestricted Access to Full Landsat Archive*, 2008 [Online]. Available: http://www.earthobservations.org/documents/pressreleases/pr_0811_bucharest_landsat.pdf

[6] *Definiens Imaging GmbH, eCognition User Guide 4,* 2004.

[7] M. Page-Jones, *The Practical Guide to Structured Systems Design*. Englewood Cliffs, NJ: Prentice-Hall, 1988.

[8] A. D. Tonchev and C. D. Tonchev, Method for Measuring the Overall Operational Performance of Hydrocarbon Facilities [Online]. Available: http://www.faqs.org/patents/app/20080262898

[9] W. Kaydos, *Operational Performance Measurement: Increasing Total Productivity*. Boca Raton, FL: CRC, 1999.

[10] P. Zamperoni, "Plus ça va, moins ça va," *Pattern Recognit. Lett.*, vol. 17, no. 7, pp. 671–677, 1996.

[11] T. Matsuyama and V. Shang-Shouq Hwang, *SIGMA-A Knowledge-based Aerial Image Understanding System*. New York: Plenum, 1990.

[12] V. Cherkassky and F. Mulier, *Learning From Data: Concepts, Theory, and Methods*. New York: Wiley, 1998.

[13] A. Strahler, D. Muchoney, J. Borak, M. Friedl, S. Gopal, E. Lambin, and A. Moody, "Modis land cover product algorithm theoretical basis document (ATBD)—Version 5.0," MODIS Science Team [Online]. Available: http://modis.gsfc.nasa.gov/data/atbd/atbd_mod12.pdf

[14] P. Mather, *Computer Processing of Remotely-Sensed Images-An Introduction*. Chichester, U.K.: Wiley, 1994.

[15] A. Baraldi, V. Puzzolo, L. Durieux, D. Simonetti, G. Conchedda, F. Holecz, and P. Blonda, "Automatic spectral rule-based preliminary classification of radiometrically calibrated SPOT-4/-5/IRS, AVHRR/MSG, AATSR, IKONOS/QuickBird/OrbView/GeoEye and DMC/SPOT-1/-2 imagery—Part I: System design and implementation, part II: Classification accuracy assessment," *IEEE Trans. Geosci. Remote Sens.*, submitted for consideration for publication, TGRS-2008-00443.R1.

[16] T. Wassenaar, A. Baraldi, and S. Kay, "Automatic preliminary spectral rule-based classification of very high resolution spaceborne imagery—Mapping vegetation and bare soils across European union's agricultural landscapes," *IEEE Trans. Geosci. Remote Sens.*, submitted for consideration for publication, TGRS-2009-00307.

[17] *GEO 2007–2009 Work Plan: Toward Convergence*, , 2008 [Online]. Available: http://earthobservations.org

[18] *The Global Earth Observation System of Systems (GEOSS) 10-Year Implementation Plan*, Feb. 16, 2005 [Online]. Available: http://www.earthobservations.org/docs/10-Year%20Implementation%20Plan.pdf

[19] A Quality Assurance Framework for Earth Observation ver. version 2.0, Sep. 2008 [Online]. Available: http://calvalportal.ceos.org/CalValPortal/showQA4EO.do?section=qa4eoIntro

[20] [Online]. Available: http://www.ceos.org.

[21] I. Dowman, "Foreword," in *International Society for Photogrammetry and Remote Sensing (ISPRS) Book Series-Post-Launch Calibration of Satellite Sensors*, S. A. Morain and A. M. Buedge, Eds. Leiden, The Netherlands: A. A. Balkema, 2004, p. IX.

[22] [Online]. Available: http://www.gmes.info.

[23] [Online]. Available: http://www.esa.int/esaLP/SEMOBSO4KKF_LPgmes_0.html.

[24] S. D'Elia, European Space Agency, Personal Communication.

[25] *IMAGE2000 and CORINE Land Cover (CLC) 2000*, , 2005, European Commission Joint Research Center, EUR 21757.

[26] E. Bartholome and A. Belward, "GLC2000: A new approach to global land cover mapping from earth observation data," *Int. J. Remote Sens.*, vol. 26, no. 9, pp. 1959–1977, 2005.

[27] M. V. N. de Lima, C. Bielski, and C. Nowak, "IMAGE2006: A component of the GMES precursor fast track service on land monitoring," in *Proc. Int. Geoscience and Remote Sensing Symp.*, Barcelona, Spain, Jul. 23–28, 2007, pp. 2669–2672.

[28] F. Achard, R. DeFries, H. Eva, M. Hansen, P. Mayaux, and H.-J. Stibig, "Pan-tropical monitoring of deforestation," *Environ. Res. Lett.*, vol. 2, pp. 1–12, 2007.

[29] [Online]. Available: http://ionia1.esrin.esa.int/index.asp.

[30] M. Herold, C. C. Woodcock, A. Di Gregorio, P. Mayaux, A. S. Belward, J. Latham, and C. Schmullius, "A joint initiative for harmonization and validation of land cover datasets," *IEEE Trans. Geosci. Remote Sens.*, vol. 44, no. 7, pp. 1719–1727, Jul. 2006.

[31] M. Kathryn and M. Korenberg, "On the use of separable Volterra networks to model discrete-time Volterra systems," *IEEE Trans. Geosci. Remote Sens.*, vol. 12, no. 1, pp. 174–175, Jan. 2001.

[32] A. Baraldi, L. Bruzzone, and P. Blonda, "Quality assessment of classification and cluster maps without ground truth knowledge," *IEEE Trans. Geosci. Remote Sens.*, vol. 43, no. 4, pp. 857–873, Apr. 2005.

[33] R. G. Congalton and K. Green, *Assessing the Accuracy of Remotely Sensed Data*. Boca Raton, FL: Lewis, 1999.

[34] G. M. Foody, "Status of land cover classification accuracy assessment," *Remote Sens. Environ.*, vol. 80, pp. 185–201, 2002.

[35] [Online]. Available: http://envisat.esa.int/handbooks/meris.

[36] *Use of the Moon for In-Flight Calibration Stability Monitoring*, GEO/CEOSS, CEOS guide: QA4EO-WGCV-IVO-CLP-001, Jul. 2008 [Online]. Available: http://calvalportal.ceos.org/CalValPortal

[37] *A Guide to Establishing a Quality Indicator on a Satellite Sensor Derived Data Product*, GEO/CEOSS, QA4EO-CEOS-GEN-DQK-001 [Online]. Available: http://calvalportal.ceos.org/CalValPortal

[38] R. R. Irish, "Landsat 7 automatic cloud cover assessment (ACCA)," in *Proc. SPIE—Algorithms Multispectral, Hyperspectral, and Ultraspectral Imagery VI*, S. S. Shen and M. R. Descour, Eds., 2000, vol. 4049, pp. 348–355 [Online]. Available: ltpwww.gsfc.nasa.gov/IAS/handbook/pdfs/ACCA_SPIE_paper.pdf

[39] S. Liang, *Quantitative Remote Sensing of Land Surfaces*. Hoboken, NJ: Wiley, 2004.

[40] P. Henry and A. Meygret, "Calibration of VEGETATION camera on-board SPOT4," *Adv. Space Res.*, vol. 28, no. 1, pp. 49–58, 2001.

[41] [Online]. Available: http://www.spotimage.fr/web/en/171-products-and-services.php.

[42] D. Riaño, E. Chuvieco, J. Salas, and I. Aguado, "Assessment of different topographic corrections in Landsat TM data for mapping vegetation types," *IEEE Trans. Geosci. Remote Sens.*, vol. 41, no. 5, pp. 1056–1061, May 2003.

[43] [Online]. Available: http://eo1.usgs.gov.

[44] T. Lillesand and R. Kiefer, *Remote Sensing and Image Interpretation*, 3rd ed. New York: Wiley, 1994.

[45] P. S. Chavez, "An improved dark-object subtraction technique for atmospheric scattering coorection of multispectral data," *Remote Sens. Environ.*, vol. 24, pp. 459–479, 1988.

[46] D. Foldes and B. Benes, "Occlusion-based snow accumulation simulation," presented at the 4th Workshop in Virtual Reality Interactions and Physical Simulation (VRIPHYS), 2007 [Online]. Available: http://www.envision.purdue.edu/pdfs/papers/Foldes07Vriphys.pdf

[47] R. Richter, Atmospheric/Topographic Correction for Satellite Imagery-ATCOR-2/3 User Guide, Version 6.2 2006 [Online]. Available: http://www.geog.umontreal.ca/donnees/geo6333/atcor23_manual.pdf

[48] C. Small, "The Landsat ETM+ spectral mixing space," *Remote Sens. Environ.*, vol. 93, pp. 1–17, 2004.

[49] G. Zhou and M. Kafatos, "Future intelligent earth observing satellites (FIEOS)," presented at the ISPRS/FIEOS Conf., 2002 [Online]. Available: http://www.isprs.org/commission1/proceedings02/paper/00031.pdf

[50] [Online]. Available: http://directory.eoportal.org/info_3rdInternationalSymposiumonFutureIntelligentEarthObservingSatellitesFIEOS.html.

[51] S. J. Russell and P. Norvig, *Artificial Intelligence: A Modern Approach*. Upper Saddle River, NJ: Prentice-Hall, 2003.

[52] M. Nagao and T. Matsuyama, *A Structural Analysis of Complex Aerial Photographs*. New York: Plenum, 1980.

[53] R. A. Brooks, "Symbolic reasoning about 3-D models and 2-D images," *Artif. Intell.*, vol. 17, pp. 285–348, 1981.

[54] D. M. McKeown, W. A. Harvey, and J. McDermott, "Rule-based interpretation of aerial imagery," *IEEE Trans. Pattern Anal. Mach. Intell.*, vol. PAMI-7, no. 5, pp. 570–585, May 1985.

[55] K. Pakzad, J. Bückner, and S. Growe, "Knowledge based Moorland interpretation using a hybrid system for image analysis," presented at the Int. Soc. Photogrammetry and Remote Sensing (ISPRS) Conf., Munich, Germany, Sep. 8–10, 1999 [Online]. Available: http://www.tnt.uni-hannover.de/papers/view.php?ind=1999&ord=Authors&mod=ASC

[56] U. Rost, H. Münkel, and C.-E. Liedtke, "A knowledge based system for the configuration of image processing algorithms," presented at the Fachtagung Informations-und Mikrosystemtechnik, Magdeburg, Germany, Mar. 25–27, 1998 [Online]. Available: http://www.tnt.uni-hannover.de/papers/view.php?ind=1999&ord=Authors&mod=ASC

[57] G. J. Hay and G. Castilla, "Object-based image analysis: Strengths, weaknesses, opportunities and threats (SWOT)," presented at the 1st Int. Conf. Object-Based Image Analysis (OBIA), Salzburg, 2006.

[58] A. K. Shackelford and C. H. Davis, "A hierarchical fuzzy classification approach for high-resolution multispectral data over urban areas," *IEEE Trans. Geosci. Remote Sens.*, vol. 41, no. 9, pp. 1920–1932, Sep. 2003.

[59] K. Shackelford and C. H. Davis, "A combined fuzzy pixel-based and object-based approach for classification of high-resolution multispectral data over urban areas," *IEEE Trans. Geosci. Remote Sens.*, vol. 41, no. 10, pp. 2354–2363, Oct. 2003.

[60] A. Baraldi, V. Puzzolo, P. Blonda, L. Bruzzone, and C. Tarantino, "Automatic spectral rule-based preliminary mapping of calibrated Landsat TM and ETM+ images," *IEEE Trans. Geosci. Remote Sens.*, vol. 44, no. 9, pp. 2563–2586, Sep. 2006.

[61] M. El Hajj, A. Begue, B. Lafrance, O. Hagolle, G. Dedieu, and M. Rumeau, "Relative radiometric normalization and atmospheric correction of a SPOT 5 time series," *Sensors*, vol. 8, pp. 2774–2791, 2008.

[62] A. Baraldi, M. Gironda, and D. Simonetti, "Operational stratified topographic correction of a remotely sensed multi-spectral image based on an automatic spectral rule-based preliminary classifier," *IEEE Trans. Geosci. Remote Sens.*, accepted for publication, TGRS-2008-00327.R1.

[63] C. Vanessa, SPOT Image, Personal Communication, Feb. 12, 2007.

[64] P. H. Swain and S. M. Davis, *Remote Sensing: The Quantitative Approach*. New York: McGraw-Hill, 1978.

[65] ENVI 4.3, User Manual ITT Industries, Inc., 2006.

[66] *A Guide to Expression of Uncertainty of Measurements*, GEO/CEOSS, QA4EO-CEOS-GEN-DQK-006 [Online]. Available: http://calval-portal.ceos.org/CalValPortal

[67] G. Chander, B. L. Markham, and D. L. Helder, "Summary of current radiometric calibration coefficients for Landsat MSS, TM, ETM+, and EO-1 ALI sensors," *Remote Sens. Environ.*, vol. 113, pp. 893–903, 2009.

[68] [Online]. Available: http://www.mcst.ssai.biz/mcstweb/performance/aqua/aqua-swir-thermal.html.

[69] *GMES IMAGE2006* [Online]. Available: http://www.gmes-gseland.info/com/news/GMES-Land_NewsLetter_I1.00.pdf.

[70] L. A. Dupigny-Giroux and J. E. Lewis, "A moisture index for surface characterization over a semiarid area," *Photogramm. Eng. Remote Sens.*, vol. 65, no. 8, pp. 937–945, Aug. 1999.

[71] *VGT4Africa User Manual*, 2006 [Online]. Available: http://www.vgt4africa.org/ViewContent.do?pageId=40, First edition, EUR 22344 EN.

[72] in *Oral Communication From A. Giros, CNES, to A. Baraldi, EC-JRC, with the Presence of S. D'Elia, ESA, and J. Inglada, CNES, During the ESA-EUSC Image Information Mining Coordination Group (IIMCG) Conference—Pursuing Automation of Geospatial Intelligence for Environment and Security*, Mar. 4–7, 2008.

[73] P. P. McLaughlin, "European technology platforms: Context, rationale and state of play," presented at the European Commission, Vilnius, Lithuania, Jul. 17, 2007.

[74] *RapidEye Image Product Specification and Price List*, Apr. 2007.

[75] [Online]. Available: http://www.esa.int/esaMI/Proba_web_site/ESARBKTHN6D_0.html.

[76] A. Belward, in *EC-JRC Mission Report, H03-IES/AB/D(2009) 517, Landsat Science Team Meeting*, Fort Collins, CO, Jan. 6–8, 2009, U.S. Forest Service.

[77] [Online]. Available: http://www.cbers.inpe.br/en/programas/p_satelites.htm.

[78] L. Durieux, Institut de Recherche Pour le. Développement, Personal Communication, Oct. 8, 2008.

[79] J. A. Barsi, B. L. Markhamb, D. L. Helderc, and G. Chanderd, "Radiometric calibration status of Landsat-7 and Landsat-5," *Proc. SPIE* [Online]. Available: http://landsat.gsfc.nasa.gov/pdf_archive/publications/SPIE07_LandsatRadiometry.pdf

[80] Y. Sohn, E. Moran, and F. Gurri, "Deforestation in North-central Yucatan (1985–1995): Mapping secondary succession of forest and agricultural land in Sotuta using the cosine of the angle concept," *Photogramm. Eng. Remote Sens.*, vol. 65, no. 8, pp. 947–958, Aug. 1999.

[81] R. Lunetta and D. Elvidge, *Remote Sensing Change Detection: Environmental Monitoring Methods and Applications*. London, U.K.: Taylor & Francis, 1999.

[82] X. Dai and S. Khorram, "The effects of image misregistration on the accuracy of remotely sensed change detection," *IEEE Trans. Geosci. Remote Sens.*, vol. 36, no. 5, pp. 1566–1577, Sep. 1998.

[83] M. Bernard, SPOT Image, Presentation at the Joint Research Center. Ispra, Italy, Jun. 12, 2008, file SPOT_6_7_.ppt.

[84] [Online]. Available: http://www.sovzond.ru/en/satellites/france/773.html.

[85] P. Roy, S. Miyatake, and A. Rikimaru, Biophysical Spectral Response Modeling Approach for Forest Density Stratification 1997 [Online]. Available: http://www.gisdelopment.net/aars/acrs/1997/tTM5/tTM5008a.shtml

[86] [Online]. Available: http://www.spotimage.fr/web/en/1822-astrium-purchases-majority-share-in-spot-image.php.

[87] [Online]. Available: http://eopi.esa.int/esa/esa.

[88] "European commission joint research center-institute for environment and sustainability," in *Proceedings and Recommendations of the Workshop on European Reference Grids*, Ispra, Italy, Oct. 27–29, 2003, 2005, EUR 21494 EN.

[89] M. Pesaresi, A. Gerhardinger, and F. Haag, "Rapid damage assessment of built-up structures using VHR satellite data in tsunami-affected areas," *Int. J. Remote Sens.*, vol. 28, no. 13 & 14, pp. 3013–3036, Jul. 2007.

[90] P. Lukowicz, E. Heinz, L. Prechelt, and W. Tichy, Experimental Evaluation in Computer Science: A Quantitative Study, Tech. Rep. 17/94 Univ. Karlsruhe, Germany, 1994.
[91] L. Prechelt, "A quantitative study of experimental evaluations of neural network learning algorithms: Current research practice," *Neural Netw.*, vol. 9, 1996.
[92] M. Pesaresi, A. Gerhardinger, and F. Kayitakire, "Monitoring settlement dynamics by anisotropic textural analysis of panchromatic VHR data," presented at the IEEE Urban Remote Sensing Joint Event, 2007.
[93] J. I. Yellott, "Implications of triple correlation uniqueness for texture statistics and the Julesz conjecture," *Opt. Soc. Amer.*, vol. 10, no. 5, pp. 777–793, May 1993.
[94] B. Julesz, "Texton gradients: The texton theory revisited," in *Biomedical and Life Sciences Collection*. Berlin/Heidelberg, Germany: Springer, Aug. 1986, vol. 54, no. 4–5.
[95] H. Anys and D.-C. He, "Evaluation of textural and multipolarization radar features for crop classification," *IEEE Trans. Geosci. Remote Sens.*, vol. 33, no. 5, pp. 1170–1181, Sep. 1995.
[96] A. Baraldi and F. Parmiggiani, "Combined detection of intensity and chromatic contours in color images," *Opt. Eng.*, vol. 35, no. 5, pp. 1413–1439, May 1996.
[97] D. Charalampidis and T. Kasparis, "Wavelet-based rotational invariant roughness features for texture classification and segmentation," *IEEE Trans. Image Process.*, vol. 11, no. 8, pp. 825–837, Aug. 2002.
[98] [Online]. Available: http://www.eomd.esa.int/booklets/pbooklet179.asp.
[99] M. Craglia, M. Goodchild, A. Annoni, G. Camara, M. Gould, W. Kuhn, D. Mark, and I. Masser, "Next-generation digital earth—A position paper from the Vespucci initiative for the advancement of geographic information science," *Int. J. Spatial Data Infrastructures Res.*, vol. 3, pp. 146–165, 2008.
[100] *Spot Image Becomes Google Earth Enterprise Partner*, September 02, 2008, Press Release [Online]. Available: http://www.directionsmag.com/press.releases/index.php?duty=Show&id=24635&trv=1
[101] IRS-P6 LGSOWG (Super Structure) Digital Data Products Format, Space Application Center, ISRO. Ahmedabad, India, May 2003 [Online]. Available: http://www.euromap.de/download/p6super_20050222.pdf
[102] *The Four Keys to Operational Performance* [Online]. Available: http://www.idii.com/wp/envistaOpPerf.pdf.
[103] Q. Yu and D. A. Clausi, "SAR sea-ice image analysis based on iterative region growing using semantics," *IEEE Trans. Geosci. Remote Sens.*, vol. 45, no. 12, pp. 3919–3931, Dec. 2007.
[104] C. Hudelot, J. Atif, and I. Bloch, "Fuzzy spatial relation ontology for image interpretation," *Fuzzy Sets Syst. Arch.*, vol. 159, no. 15, pp. 1929–1951, Aug. 2008.
[105] T Esch, M. Thiel, A. Roth, and S. Dech, "Improvement of image segmentation accuracy based on multiscale optimization procedure," *IEEE Geosci. Remote Sens. Lett.*, vol. 5, no. 3, pp. 463–467, Jul. 2008.
[106] P. Corcoran and A. Winstanley, "Using texture to tackle the problem of scale in landcover classification," in *Object-Based Image Analysis - Spatial concepts for knowledge-driven remote sensing applications,* T. Blaschke, S. Lang, and G. Hay, Eds., pp. 113–132, 2007, Springer Lecture Notes in Geoinformation and Cartography.
[107] M. Petrou and P. Sevilla*, Image processing: Dealing with Texture*. Chinchester, U.K.: Wiley, 2006.

Andrea Baraldi was born in Modena, Italy, in 1963. He received the Laurea (M.S.) degree in electronic engineering from the University of Bologna, Italy, in 1989. His M.S. thesis focused on the development of segmentation and classification algorithms for remotely sensed optical imagery.

From 1989 to 1990, he worked as a research associate at CIOC-CNR, an Institute of the National Research Council (CNR) in Bologna, and served in the army at the Istituto Geografico Militare in Florence, working on satellite image classifiers and geographic information systems (GIS). As a consultant at ESA-ESRIN, Frascati, Italy, he worked on object-oriented applications for GIS from 1991 to 1993. From Dec. 1997 to June 1999 he was assigned with a postdoctoral fellowship in Artificial Intelligence at the International Computer Science Institute, Berkeley, CA. From 2000 to 2002, as a postdoctoral researcher, he joined the Global Vegetation Monitoring unit of the Institute for Environment and Sustainability (IES) of the European Commission Joint Research Centre (JRC), Ispra, Italy, in the development and validation of classification algorithms of radar mosaics for continental scale mapping of forest ecosystems. From 2005 to 2009, at the IES-Spatial Data Infrastructure (SDI) unit of the JRC, he was involved with satellite optical image enhancement, classification, and mosaicking at continental scale. Since his M.S. thesis, he has continued his collaboration with ISAC-CNR in Bologna and ISSIA-CNR in Bari, Italy. His main interests center on image understanding, with special emphasis on the development of fully automated hierarchical multisource, multiresolution spaceborne image understanding systems consistent with biological vision.

Mr. Baraldi served as an Associate Editor of the IEEE TRANSACTIONS ON NEURAL NETWORKS from 2001 to 2006.